

The Islamic University Gaza
Higher Education Deanship
Faculty of Engineering
Civil Engineering Department
Design and Rehabilitation of Structures



الجامعة الإسلامية - غزة
عمادة الدراسات العليا
كلية الهندسة
قسم الهندسة المدنية
تأهيل وتصميم المنشآت

نمذجة التفاعل المتبادل ما بين المائع والمنشأ لعמוד فردي معرض لأحمال الأمواج

Fluid Structure Interaction Modeling of a Monopile Subjected to Wave Load

Submitted by:

Hussein A AliHussein

Supervised by:

Dr. Mohammed Arafa

Dr. Mamoun Alqedra

A Thesis Submitted in Partial Fulfillment of Requirements for the Degree of Master of
Science in Civil Engineering

Design and Rehabilitation of Structures

2014

نموذج رقم (1)

إقرار

أنا الموقع أدناه مقدم الرسالة التي تحمل العنوان:

مذكرة لتفاعل المتبارل مايسه الماسخ والمث للعلوم فزي مرمه لأعلان الأمواع

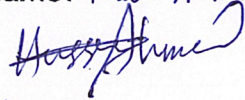
أقر بأن ما اشتملت عليه هذه الرسالة إنما هو نتاج جهدي الخاص، باستثناء ما تمت الإشارة إليه حيثما ورد، وإن هذه الرسالة ككل أو أي جزء منها لم يقدم من قبل لنيل درجة أو لقب علمي أو بحثي لدى أي مؤسسة تعليمية أو بحثية أخرى.

DECLARATION

The work provided in this thesis, unless otherwise referenced, is the researcher's own work, and has not been submitted elsewhere for any other degree or qualification

Student's name: Hussein Althusein

اسم الطالب: حسين المرسي / علي

Signature: 

التوقيع: 

Date: 31/8/2014

التاريخ: 31/8/2014



نتيجة الحكم على أطروحة ماجستير

بناءً على موافقة شئون البحث العلمي والدراسات العليا بالجامعة الإسلامية بغزة على تشكيل لجنة الحكم على أطروحة الباحث/ حسين أحمد حسين علي حسين لنيل درجة الماجستير في كلية الهندسة قسم الهندسة المدنية - تصميم وتأهيل المنشآت وموضوعها:

نمذجة التفاعل المتبادل ما بين المائع والمنشأ لعامود فردي معرض لأحمال الأمواج Fluid Structure Interaction Modeling of a Monopile Subjected to Wave Load

وبعد المناقشة التي تمت اليوم السبت 16 شعبان 1435هـ، الموافق 2014/06/14م الساعة العاشرة صباحاً، اجتمعت لجنة الحكم على الأطروحة والمكونة من:

.....
.....
.....
.....

د. محمد حسني عرفة مشرفاً ورئيساً
د. مأمون عبد الحميد القدرة مشرفاً
د. جمال محمد سعيد/الزبدة مناقشاً داخلياً
د. مازن طه أبو الطيف مناقشاً داخلياً

وبعد المداولة أوصت اللجنة بمنح الباحث درجة الماجستير في كلية الهندسة/ قسم الهندسة المدنية -

تصميم وتأهيل المنشآت.

واللجنة إذ تمنحه هذه الدرجة فإنها توصيه بتقوى الله ولزوم طاعته وأن يسخر علمه في خدمة دينه ووطنه.

والله ولي التوفيق،،،

مساعد نائب الرئيس للبحث العلمي والدراسات العليا

أ.د. فؤاد علي العاجز
014
010
Research & Graduate Affairs

DEDICATION

I would like to dedicate this thesis to my mother and father, without their support, I would have not achieved this thesis. As well, I dedicate this thesis to my beloved wife, Hadil, who did more than possible to help as I sat at the computer working on this thesis. To my little son, Ahmed, who brings happiness and joy to me each time I look at him.

ACKNOWLEDGEMENT

I am profoundly indebted to my supervisors, Dr. Mohammed Arafa and Dr. Mamoun Alqedra, who were very generous with their time and knowledge and assisted me in each step to complete the thesis.

Many thanks also to those who helped arrange the field work for me, especially my friend Mohammed Ashour. Finally, but not least, thanks go to my whole family who have been an important and indispensable source of spiritual support.

ملخص الدراسة

في هذه الأطروحة تم بناء نموذج عددي يعتمد مبدأ التفاعل بين المائع والهيكلي، لدراسة تأثير أمواج البحر على العناصر الإنشائية المستخدمة في المنشآت البحرية، وتم التحقق من نتائج النموذج العددي عبر مقارنتها بنتائج نموذج رياضي تحليلي. يستند النموذج العددي على معادلات نافيه ستوكس التي تصف تصرف الموائع، تم استخدام برنامج حاسوبي ANSYS CFX لديه المقدرة على حل معادلات نافيه ستوكس للنموذج قيد الدراسة باستخدام طريقة عددية هي طريقة الحجم المحدود. النموذج قيد الدراسة يحتوي أكثر من مائع: الماء والهواء وبالتالي لزم تحديد شكل ومكان السطح الحر، برنامج ANSYS CFX يستخدم طريقة حجم السوائل لتحديد شكل ومكان السطح الحر.

لتوفير الجهد الحسابي، وللوصول إلى النتائج المرغوبة بشكل أسرع، تم اعتماد توجيهات الباحثان (فينيجان وجوجينز، 2012) لبناء النموذج العددي الأمثل من حيث اختيار أقل أبعاد ممكنة للنموذج باستخدام ANSYS CFX دون التأثير على النتائج، وأيضا اختيار حجم العناصر المستخدمة في الشكل الشبكي الذي يستخدم في الحل العددي.

تم بناء خمسة نماذج لدراسة تصرف الأمواج وتأثيرها على المنشآت، النموذج الأول وهو نموذج ثنائي الأبعاد استخدم للتأكد من استطاعة برنامج ANSYS CFX نمذجة حوض الأمواج العددي، حيث تم الاستناد في بنائه على توصيات الباحث (سيلفا، 2010) وباقي الأربعة نماذج استخدمت لمعرفة القوى المؤثرة على المنشأ حيث احتوى كل منها على عامود كابولي يختلف في الطول وفي شكل المقطع، وذلك لدراسة تأثير تغيير هذه المتغيرات في النتائج. تم توليد الأمواج عدديا باستخدام (مولد أمواج) من نوع (المكبس)، يخضع لنظرية (مولد الأمواج)، في كل من النماذج الخمس.

فيما يتعلق بالنماذج المحتوية على المنشأ، احتوى النموذج الأول على عامود ذو مقطع دائري 0.5 متر ويبلغ ارتفاعه 4.35 مترا، أما النموذج الثاني فقد احتوى على عامود بنفس شكل المقطع لكن بطول 3.25 متر، النموذجين الثالث والرابع احتويا على عامود مربع المقطع بطول ضلع 0.5 مترا، ويطول 4.35 متر و3.25 مترا بالترتيب، حيث تمت مقارنة تأثير هذه الاختلافات على القوى المؤثرة على كل من الأعمدة.

النتائج المستقاة من النموذج -الخاص بالتأكد من مقدرة CFX على تمثيل الأمواج عدديا- بيّنت اتفاقا في شكل الموجة المولدة بين الحل التحليلي (نظرية الأمواج الخطية)، والحل العددي باستخدام CFX، حيث اتفقت الموجتان في ارتفاع السطح الحر، وفي التردد.

لوحظ وجود اتفاق في النموذج الأول بين النتائج العددية والتحليلية فيما يتعلق بارتفاع سطح الموجة، وشكلها وكذلك ترددها، أما بالنسبة للقوى والعزوم المؤثرة على العامود في النموذج الأول فقد أعطى الحل العددي قيمة أكبر من الحل التحليلي.

في النموذج الثاني لم يختلف الأمر كثيرا عن النموذج الأول وكانت نتائج التحليل مقارنة جدا نظرا لعدم وجود قوة ذات قيمة مؤثرة من قبل الرياح تؤدي إلى وجود اختلاف في النتيجة.

في النموذج الثالث كانت النتيجة مقارنة جدا للحل العددي وشبه مطابقة له، نتيجة الشكل المربع لمقطع العامود والذي له معامل سحب أكبر أدى إلى ارتفاع قيمة القوى والعزوم المؤثرة عليه.

في النموذج الرابع كانت النتائج مشابهة للنموذج الأول واتفق ارتفاع سطح الموجة والقوى والعزوم المؤثرة على العامود في الحلين العددي والتحليلي، مع وجود فارق بسيط في القيمة بسبب وجود تداخل بين السطح الحر والعامود.

ABSTRACT

Offshore monopile foundations are one of the most commonly used foundation structures, especially in areas with relatively shallow water. One of the most significant aspects is associated with the wave effect on the structural behavior of monopile foundations.

In this work, a developed numerical method for water-wave body interaction was used to study the water wave's effects on the structural behavior of the monopiles. A validation procedure was conducted by comparing the numerical results with analytical wave mathematical model results. The numerical model is based on Reynolds Averaged Navier Stokes equations (RANS) considering the effects of energy dissipation. ANSYS CFX was used to solve (RANS) using finite volume method. The free surface displacements are tracked by the volume of fluid method. The numerical model is used to simulate periodic first order waves and their interaction with a vertical slender monopile. The geometry and mesh of the numerical model were optimized using the guidelines of Finnegan and Goggins (2012) [1] to save the computational effort.

Five models were built in this study to obtain the behavior of waves and their effect on structures. The first model is a bi-dimensional model used to test the ability of ANSYS CFX to simulate Numerical Wave Tanks accurately; a piston wavemaker is created to generate waves according to the recommendations of Silva et al. (2010) [2] for this model. The rest of the four models used to determine the forces acting on the studied structures, where each of them contained a monopile of different length and cross section.

The first and second models represented a monopile of length 4.35m and 3.25m, respectively with a cross section of a circle with a diameter of 0.5m, whereas the third and fourth models represented a monopile of the same length and a cross section of a square with a side length of 0.5m.

Very good agreement between the analytical results and numerical results are observed for the time history of free surface displacement, hydrodynamic forces and moments on the monopile.

LIST OF CONTENTS

1	CHAPTER 1: INTRODUCTION	1
1.1	Problem Statement	1
1.2	Research Aim.....	1
1.3	Research Objectives	2
1.4	Brief Research Methodology	2
1.5	Research Importance	3
1.6	Research Scope and Limitations	4
1.7	Thesis contents.....	4
2	CHAPTER 2: BACKGROUND REVIEW	5
2.1	Wave Modeling.....	5
2.1.1	Analytical wave modeling.....	5
2.1.2	Empirical wave modeling	5
2.1.3	Physical wave modeling (Prototype).....	6
2.1.4	Numerical wave modeling	6
2.2	Classification of Seawater Waves.....	7
2.3	Numerical Models for Water Waves.....	7
2.3.1	Wave spectral models	8
2.3.2	Mild-slope equation wave models.....	8
2.3.3	Boussinesq equation wave models.....	9
2.3.4	Shallow-water equation wave models.....	9
2.3.5	Quasi-three-dimensional hydrostatic pressure wave models	9
2.3.6	Fully three-dimensional wave models with turbulence: Navier-Stokes equation models	10
2.3.7	Fully three-dimensional wave models without turbulence: potential flow models.	11
2.4	Previous Studies.....	11
3	CHAPTER 3: THEORITICAL BACKGROUND	14
3.1	Computational Fluid Dynamics (CFD).....	14
3.2	CFD Theory	16
3.2.1	Conservation of mass	16
3.2.2	Conservation of momentum.....	17
3.2.3	Conservation of energy	19
3.2.4	Discretization using ANSYS CFX.....	19

3.2.5	Turbulence models	20
3.2.6	Free surface	24
3.2.7	Overview of domain boundary conditions	26
3.3	Potential Wave Theory.....	28
3.4	Breaking Wave.....	30
3.5	Wavemaker Theory	30
3.6	Morison's Equation.....	33
4	CHAPTER 4: NUMERICAL MODEL SETUP	36
4.1	Numerical Wave Tank	36
4.2	Developing the Numerical Model	37
4.2.1	Domain and meshing.....	37
4.2.2	Numerical settings.....	40
4.2.3	Producing waves at the inlet.....	42
4.2.4	Boundary conditions and numerical settings	43
4.2.5	CFX Expression Language	45
4.3	Validation Procedure (2D NWT without a monopile)	45
4.4	Identification of the Numerical Settings of the Proposed NWT	47
5	CHAPTER 5: COMPUTATIONS, RESULTS AND DISCUSSION.....	50
5.1	Results and Discussion.....	50
5.1.1	Wave free surface elevation	50
5.1.2	Force and moment measurement.....	51
5.1.3	Results of case one: long circular-cross section monopile.....	51
5.1.4	Results of case two: short circular-cross section monopile.....	55
5.1.5	Results of case three: long square-cross section monopile	58
5.1.6	Results of case four: short square-cross section monopile.....	61
5.2	Effect of monopile length on total hydrodynamic forces.....	64
5.3	Effect of monopile cross section on total hydrodynamic forces	66
5.4	Comparison of the free surface elevation of the four cases	67
6	CHAPTER 6: CONCLUSION AND RECOMMENDATIONS.....	68
6.1	Modeling of the NWT	68
6.2	Conclusion	68
6.3	Recommendations	69

LIST OF ABBREVIATIONS

CFD	Computational Fluid Dynamics
FSI	Fluid Structure Interaction
NWT	Numerical Wave Tank
NSE	Navier Stokes Equations
SWL	Sea Water Level
VOF	Volume of Fluid
WMT	Wave Maker Theory

LIST OF TABLES

Table 4.1 Density and viscosity of water and air.....	40
Table 4.2 General numerical Settings.....	41
Table 4.3 Domain and mesh properties	43
Table 4.4 Numerical settings for the four cases.....	49
Table 4.5 Wave input parameters	49

LIST OF FIGURES

Figure 1.1 Progression of fixed platforms in the Gulf of Mexico - depths in meters, [4]	3
Figure 1.2 Slender cylindrical structures in coastal and offshore Engineering, [5].....	3
Figure 2.1 Littoral zone classification[8].....	7
Figure 3.1 The different disciplines contained within computational fluid dynamics ...	14
Figure 3.2 The three basic approaches to solve problems in fluid dynamics	15
Figure 3.3 Velocity fluctuating with time at some point in a turbulent flow [15].....	20
Figure 3.4 Boundary layer showing the sub layer, logarithmic layer and the buffer layer. ANSYS (2013).....	22
Figure 3.5 Water fraction.....	25
Figure 3.6 An exaggerated view of three inflation layers on each side of the uppermost subdomain boundary surface [38].....	26
Figure 3.7 Wave characteristics [41]	29
Figure 3.8 Definition of wave height and wave length.....	30
Figure 3.9 Simplified shallow water piston-type wavemaker theory of Galvin [41]	31
Figure 3.10 Wave height to stroke ratios versus relative depths from plane wavemaker theory [41].....	33
Figure 3.11 The force components of Morison equations	34
Figure 4.1 The three main elements of a CFD code	37
Figure 4.2 Geometry of the model.....	38
Figure 4.3 The NWT of Mo et al.[5]	40
Figure 4.4 Domain dimensions	42
Figure 4.5 Bottom-hinged flap wavemaker	43
Figure 4.6 Piston wavemaker.....	43
Figure 4.7 Mesh in case one	44
Figure 4.8 Model boundary conditions.....	45
Figure 4.9 The NWT for the validation case	46
Figure 4.10 Silvia NWT Numerical vs. Analytical Wave Profile Solution $h=1.5\text{m}$, $L=6\text{m}$ at $t= 60\text{ sec}$	47
Figure 4.11 Domain of the first case. Similar domain was used for the other three cases.	48
Figure 5.1 Model with the plane used to monitor wave elevation at $x=11\text{m}$ away from the wavemaker is shown.....	50
Figure 5.2 Geometry of the first case	51
Figure 5.3 Mesh in case one	52
Figure 5.4 Free surface elevation for Case 1 compared with Linear wave theory, measured at $x=11\text{ m}$ from the wavemaker	53
Figure 5.5 Comparison of total force acting on monopile for Case1 between CFD and Morison's equation.....	54
Figure 5.6 Comparison of total moment around seabed acting on monopile for Case 1 between CFD and Morison's equation	54
Figure 5.7 Geometry of the second case.....	55
Figure 5.8 Mesh in case two	56
Figure 5.9 Free surface elevation for Case 2 compared with Linear wave theory, measured at $x=11\text{ m}$ from the wavemaker	57

Figure 5.10 Comparison of total force acting on monopile for Case 2 between CFD and Morison's equation.....	57
Figure 5.11 Comparison of total moment about seabed acting on monopile for Case 2 between CFD and Morison's equation	58
Figure 5.12 Geometry of the third case	58
Figure 5.13 Mesh in case three	59
Figure 5.14 Free surface elevation for Case 3 compared with Linear wave theory, measured at x=11 m from the wavemaker.....	60
Figure 5.15 Comparison of total force acting on monopile for Case 3 between CFD and Morison's equation.....	60
Figure 5.16 Comparison of total moment about seabed acting on monopile for Case 3 between CFD and Morison's equation	61
Figure 5.17 Geometry of the fourth case	61
Figure 5.18 Mesh in case four	62
Figure 5.19 Free surface elevation for Case 4 compared with Linear wave theory, measured at x=11 m from the wavemaker.....	63
Figure 5.20 Comparison of total force acting on monopile for Case 4 between CFD and Morison's equation.....	63
Figure 5.21 Comparison of total moment about seabed acting on monopile for Case 4 between CFD and Morison's equation	64
Figure 5.22 Forces on long and short Circular Monopiles	64
Figure 5.23 Forces on long and short Square Monopiles	65
Figure 5.24 Forces distribution on case I monopile.....	65
Figure 5.25 Forces distribution on case II monopile	66
Figure 5.26 Velocity streamlines and vectors around circular monopile at elevation=2.5m, time= 9.6 s.....	66
Figure 5.27 Velocity streamlines and vectors around square monopile at elevation=2.5m, time= 9.6 s.....	67
Figure 5.28 Comparison of the free surface elevation in the four cases at x=11m	67

1 CHAPTER 1: INTRODUCTION

Numerical simulation using computers or computational simulation has increasingly become a very important approach for solving complex practical problems in engineering and science. Numerical simulation translates important aspects of a physical problem into a discrete form of mathematical description, recreates and solves the problem on a computer, and reveals phenomena virtually according to the requirements of the analysts. Rather than adopting the traditional theoretical practice of constructing layers of assumptions and approximations, this modern numerical approach attacks the original problems in all its detail without making too many assumptions, utilizing the increasing computer power.

In general, computation of wave loads on structures is complicated by the complex nature of wave-structure interaction. Because structure in water interrupts the propagation of waves, the flow field associated with waves depends on both wave conditions and the structure geometry[3].

1.1 Problem Statement

Offshore monopiles, as an important foundation concept, have been increasingly receiving attention of scientists and engineers. Generally, embedded in shallow waters with a depth of no more than 50 m, offshore monopiles have a much larger diameter than those of other pile foundations

Ocean waves impose cyclic and detrimental loads on monopiles during their entire operational lifetime, and therefore, are considered as predominant factors when analyzing monopile behavior[4].

Unfortunately, there is no established technical guideline for offshore monopile design and construction that can be universally applied due to its environmental-dependent nature. [4]

1.2 Research Aim

The main goal of this work is to develop a numerical model, known as a numerical wave tank, which can replicate the behavior of waves in an experimental wave tank. This NWT will be used for obtaining loads on monopiles caused by water waves. The numerical

wave tank will be created using a computational fluid dynamics (CFD) software known as ANSYS CFX, which allows the simulation, and determination of forces and wave actions before physical construction takes place.

1.3 Research Objectives

Within the main goal of the thesis, there are several objectives, which can be summarized as follows.

1. Constructing a NWT using ANSYS CFX, with optimum dimensions and meshing to save computational effort. This NWT will be used for the purpose of modeling the problem of wave-structure interaction.
2. Producing regular waves (linear waves) within the proposed NWT.
3. Validating the behavior of the waves produced from the NWT against the analytical solution of linear wave's theory.
4. Obtaining the results of wave's forces and moments acting on the proposed structures (i.e. monopiles) from the NWT.
5. Validating forces and moments obtained from CFX against Morison's equation.

1.4 Brief Research Methodology

In this study, a numerical model will be developed to explore the monopile response to sea waves and the interaction between them. The model is set for the benefit of subsequent investigation on the effect of monopile cross section shape and length on its behavior when it is exposed to seawater loads.

A typical monopile is associated with three physical aspects according to the spatial division by the medium surrounding it, i.e., aerodynamically with the wind, hydrodynamically with the seawater, and geotechnically with the seabed. There are also static loads transferred and act on the monopile. These aspects are not considered due to the intensive objective of this study, which mainly focuses on the wave loads and the resulting structural response of the monopile.

A model for predicting the interaction of fluid with structures will be introduced in this work, which is a complex problem due to the interaction of the nonlinear fluid behavior with the structural behavior.

A set of simulations will be performed to demonstrate the structural response due to water impact; hence, a parametric study has been carried out using key parameters such as monopiles section shape and monopile height, which are of great significance to the monopile behavior.

1.5 Research Importance

The usage of offshore structures have been developing since the last half-century, see Figure 1.1, due to the usage of these structures for plenty of reasons.

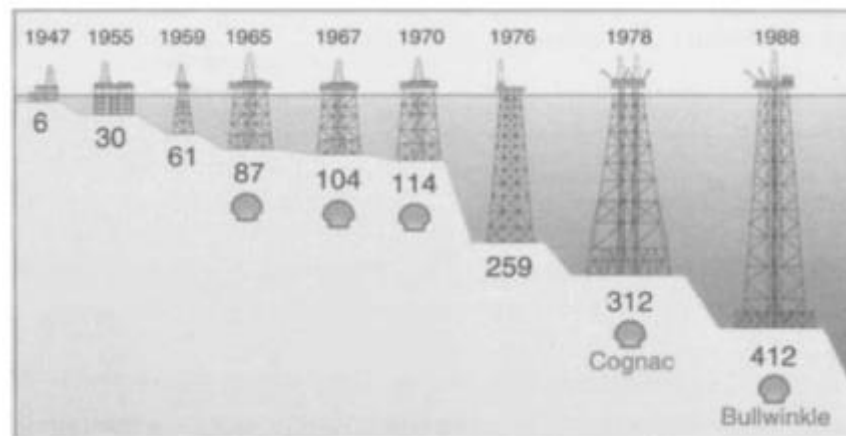


Figure 1.1 Progression of fixed platforms in the Gulf of Mexico - depths in meters, [4]

While the majority of offshore structures support the exploration and production of oil and gas, other major structures e.g. for harnessing power from sea, offshore bases, offshore airports are also coming into existence, see Figure 1.2.

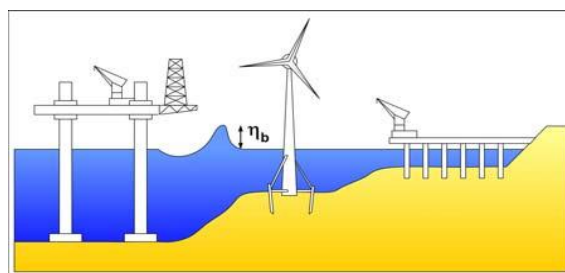


Figure 1.2 Slender cylindrical structures in coastal and offshore Engineering, [5]

Gaza Strip, one of the most densely populated areas in the world. It suffers from two main problems: the problem of lack of space, and the problem of the scarcity of energy sources;

this has led to power outages for long periods during the past years. The previous two problems require finding creative solutions; one of the options is to resort to the sea to expand and to reap the energy. Such solutions requires knowledge of the impact of the waves on marine structures.

1.6 Research Scope and Limitations

Only numerical wave tanks implementing regular waves are considered within this thesis. There are numerous studies that uses NWTs implement solitary, or other irregular waves, but the production of these waves is outside the scope of this thesis.

1.7 Thesis contents

This thesis is divided into five chapters. The first and current chapter outlines the objectives and motivation underlying the work.

The second chapter introduces literature related to numerical wave tank research and outlines the experiments used to validate the developed numerical wave tank.

The third chapter summarizes the governing equations of the fluid behavior and ANSYS CFX source code are presented.

Chapter four discusses the methodology used to create the numerical wave tank. The modelled geometry is presented, along with simulation parameters, wave parameters and detailed discussion of creating the inlet boundary condition and preventing reflection of waves from the outlet.

Chapter five presents the results of the various simulations outlined in chapter four. Analytical validation of the numerical wave tank is presented as well.

Chapter six presents the limitations of the simulation and the recommendation for future work.

2 CHAPTER 2: BACKGROUND REVIEW

2.1 Wave Modeling

There are various types of techniques for modeling a prototype wave system, i.e., analytical wave modeling, empirical wave modeling, physical wave modeling, and numerical wave modeling. With their inherent advantages and limitations, these techniques shall be applied for different purposes.

2.1.1 Analytical wave modeling

A physical wave system in nature can be very complicated. A way to represent the wave system by analyzing the system with a simplified theoretical model that should be able to capture the most important characteristics of the wave system. The model is usually expressed by mathematical equations, which are in the form of partial differential equations (PDEs) or ordinary differential equations (ODEs) governing the space-time relationship of the important variables for the waves.

A good theoretical model is always constructed on rigorous mathematical derivations, each step of which has clear physical and mathematical assumptions and implications. When the equations are solved analytically for a specific condition, the closed-form solution can be obtained and used to predict wave system behavior accurately. This procedure of solution seeking is called analytical wave modeling, which is a powerful tool for us to understand the physical phenomenon of a particular wave system.

One typical example of this kind of modeling is the wave-scattering pattern around a large vertical circular cylinder with the use of diffraction theory. Unfortunately, although most of the wave systems can be formulated theoretically, only very few of them can be solved analytically. This greatly limits the application of this approach to general wave problems[3].

2.1.2 Empirical wave modeling

An empirical formula is usually a simple mathematical expression summarized from available field data of a prototype system. It can describe the system behavior in terms of simple algebraic equations with important parameters. Since the empirical approach is simple and easy to implement, it is widely adopted in engineering design. In empirical

wave modeling, empirical formulas can be used to estimate the maximum wave load on a structure (i.e., the Morison equation), the reflection coefficient from a certain type of structure, the maximum wave run-up on a beach, and the maximum wave overtopping rate over a dike. However, since empirical formulas are established on the known problems and database, when a new prototype system is considered, the existing empirical formulas may not be suitable[3].

2.1.3 Physical wave modeling (Prototype)

To understand a prototype wave system in nature, alternatively a small-scale physical model can be built in the laboratory as a prototype. The wave characteristics (and wave loads on the model structure if wave-structure interaction is investigated) can be obtained by laboratory measurements. The information can then be extrapolated based on certain scaling laws to estimate what will really happen to the prototype system.

This approach is called physical wave modeling. It is straightforward and allows us to visualize and understand the important physical processes from the small-scale model study. Typical examples of physical wave modeling include the studies of wave loads on an offshore structure, wave transmission and reflection from a breakwater, etc. However, when a physical system becomes very complicated, a physical model that satisfies all the important scaling laws, on which the physical model is designed and constructed, may not exist. Under such circumstances or when a physical model study is too expensive and time-consuming other approaches may have to be sought. Readers are referred to Hughes (1993) [6] for a more detailed description of the physical models in coastal engineering and to Chakrabarti (1994) [7] for offshore structure modeling.

2.1.4 Numerical wave modeling

A numerical wave model is the combination of the mathematical representation of a physical wave problem and the numerical approximation of the mathematical equations. Compared to analytical modeling, the difference is only in the means of finding the solution of the governing equations for the wave problems. To model ocean waves numerically, it must be started from some existing “wave equations” obtained from theoretical studies. In most cases, more than one wave equation is there to describe the same wave phenomenon, depending on different levels of approximation made in the

theoretical derivations. Similarly, the same wave model can also be applied to many different wave problems, as long as the basic assumptions in the model are valid.

2.2 Classification of Seawater Waves

The seawater waves are classified according to the water depth to three main zones, as shown in Figure 2.1 [8]:

- The onshore zone: the depth of water varies from 0m to 10m.
- The nearshore zone: the depth of water varies from 10m to 50m.
- The offshore zone: the depth of water is over 50m.

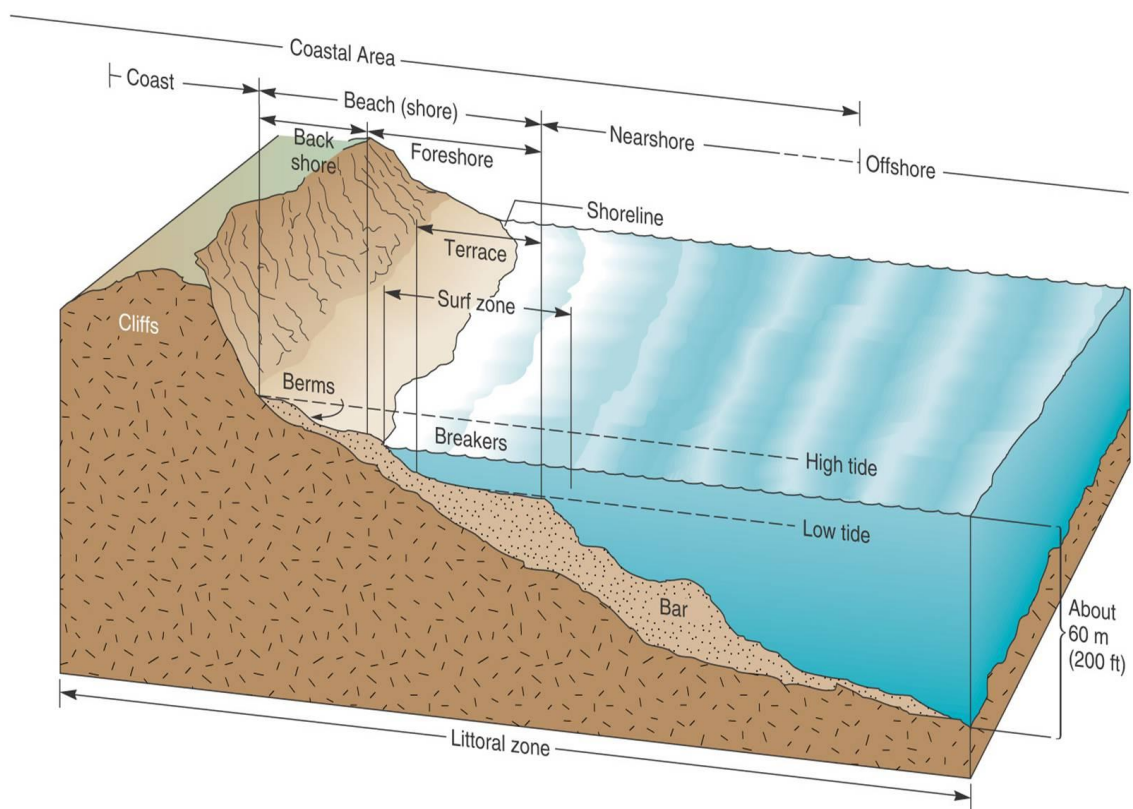


Figure 2.1 Littoral zone classification[8]

2.3 Numerical Models for Water Waves

In the following subsections, classification for wave models based on their modeling capability is presented.

2.3.1 Wave spectral models

The most commonly employed wave model in modeling large-scale wave motion is the wave energy spectral model or wave action spectral model. This type of model is constructed on the assumption that a random sea state is composed of an infinite number of linear waves whose wave height is a function of wave frequency and the direction of wave propagation.

The representative wave energy spectral models are WAM (Wave Prediction Model) Hasselmann, et al. (1988) [9] and Wavewatch III Tolman (1999)[10], which can be used to model large-scale variations of wave heights in deep oceans. Being connected with an atmosphere model, a wave energy spectral model is able to predict global ocean wave climate. When the current effect is considered, the wave action spectral model can be formulated and used instead to simulate combined wave-current interaction in a large-scale nearshore region, see Ris, et al. (1999)[11].

With the wave phase information being filtered out in the formulation, the wave spectral model can use computational meshes much larger than a wavelength and thus can be applied in a very large area. Without wave phase information, however, the model is unable to represent wave diffraction that is phase-related. For this reason, this kind of model is usually used to provide far-field wave information only. The detailed wave pattern around coastal structures where diffraction is important is left to other types of wave models.

2.3.2 Mild-slope equation wave models

The mild-slope equation (MSE) was originally derived based on the assumptions of linear waves and slowly varying bottoms. The equation can be used to describe combined wave refraction and diffraction in both deep and shallow waters. In most events, the MSE model is employed to study monochromatic waves, though it can be applied to irregular waves by summing up different wave harmonics. The extension of the MSE to abruptly varying topography and larger amplitude waves was also attempted in the last two decades. So far, most of the applications of the MSE models are limited to the region from an offshore location to a nearshore location some distance away from the shoreline before wave nonlinearity becomes strong.

One exception is its application in harbor resonance modeling because water depth in a harbor is usually deep even along the boundaries. The MSE has three different formulations, namely the hyperbolic MSE for a time-dependent wave field, the elliptic MSE for a steady-state wave field, and the parabolic MSE for a simplified steady-state wave field that has a primary wave propagation direction, see Eckart (1952)[12].

2.3.3 Boussinesq equation wave models

To model nearshore waves with strong wave nonlinearity, a Boussinesq equation wave model (or simply the Boussinesq model in water wave modeling) is often a good choice. The Boussinesq equations are depth-averaged equations with the dispersion terms partially representing the effect of vertical fluid acceleration.

Rigorously speaking, Boussinesq equations are valid only from intermediate water depth to shallow water before the waves break. However, in engineering applications, the equations are often extended beyond the breaking point, up to wave run-up in the swash zone. This is possible by adding an artificial energy dissipation term for wave breaking. Besides, efforts are also made to extend the model to deeper water. Unlike the wave spectral model and the MSE model, the Boussinesq model does not have the presumption that the flow is periodic. Therefore, it can be applied to waves induced by impulsive motions, i.e., solitary waves, landslide-induced waves, tsunami, and unsteady undulation in open channels Dingemans (1997) [13]

2.3.4 Shallow-water equation wave models

To model tsunami or other long waves (e.g., tides), a shallow-water equation (SWE) model is more likely to be adopted. Compared with the Boussinesq model, the SWE model is simpler because the flow is assumed to be uniform across the water depth and the wave-dispersive effect is neglected. The SWE model has a wide application range in modeling tsunami, tides, storm surges, and river flows. The main limitation of the SWE model is that it is suitable only for flows whose horizontal scale is much larger than vertical scale, see Randall (2006)[14].

2.3.5 Quasi-three-dimensional hydrostatic pressure wave models

All the earlier discussed wave models can be operated on a horizontally two-dimensional (2D) plane due to vertical integration. When a shallow-water flow is modeled, the depth-

varying information may still be needed on some occasions. A typical example is ocean circulation where the horizontal length scale is much larger than the vertical scale, but the vertical circulation, though relatively weak, is still of interest in many events. Thus, in this case, a three-dimensional (3D) model would be necessary. This type of model often solves the 3D Navier-Stokes equations (NSEs) directly under the hydrostatic pressure assumption. Under such an assumption, the solution procedure to the 3D NSEs is greatly simplified and the model is referred to as the quasi-3D model, against the fully 3D model to be discussed later. The model of this type is often solved in the σ -coordinate that maps the irregular physical domain to the regular computational domain for the ease of application of the boundary condition. The representative model of this kind is the Princeton Ocean model (POM) Pengzhi (2008)[3].

2.3.6 Fully three-dimensional wave models with turbulence: Navier-Stokes equation models

To model fully 3D wave problems, a turn to the general governing equations, NSEs is necessary, without a hydrostatic pressure assumption. The NSEs are derived from the general principle of mass and momentum conservation that is able to describe any type of fluid flow including water waves. With the inclusion of a proper turbulence model, it is possible for an NSE model to simulate difficult wave problems, e.g., nonbreaking or breaking waves, wave-current interactions, and wave-structure interactions. When breaking waves are simulated, there is the potential to include air entrainment on the surface of the water; when the wave-body interaction is computed, it can treat both the rigid body and the flexible body. With almost no theoretical limitation, this type of model seems to be the best choice of all. However, the main barrier that prevents the wide application of such a model is the expensive computational effort. To solve the fully 3D NSEs, the computation can be much more expensive than all the previously introduced wave models. So far, the application of such models in engineering computation is still restricted to the simulation of local wave phenomena near the location of interest, e.g., the surf zone when the breaking wave and/or sediment transport is considered and the flows around coastal and offshore structure when the wave-structure interaction is considered, refer to Tu, et al. (2008)[15].

2.3.7 Fully three-dimensional wave models without turbulence: potential flow models

When turbulence is negligible and the bottom boundary layer thickness is thin (e.g., nonbreaking waves), the NSEs can be reduced to the Laplace equation based on potential flow theory. The theory is applicable to most of the linear and nonlinear nonbreaking waves and their interaction with large bodies. The Laplace equation can be solved numerically by many different methods. One of the most commonly used methods is the boundary element method (BEM), which converts domain integration into surface integration with the use of Green's theorem. This type of model is capable of simulating highly nonlinear waves in both deep and shallow waters. It is effective in the study of nonlinear wave transformation over changing topography, linear wave diffraction over a large body, and wave force on a large structure. The major limitation of such a model lies on the potential flow assumption that requires the flow to be irrotational. For this reason, the model is unable to simulate breaking waves as well as wave interaction with small bodies, during which the flow becomes rotational. Furthermore, the computational cost for modeling 3D fully nonlinear waves using BEM is rather high Pengzhi (2008)[3].

2.4 Previous Studies

The accurate modeling of the behavior of water waves is an important subject for the field of coastal and ocean engineering. As computational power has increased, numerical models and numerical wave tanks (NWT) have become an increasingly viable option for the modelling of surface water waves.

Numerical wave tanks can be achieved through the creation of a numerical model or with an existing program, such as ANSYS CFX, as was done for this work. The use of an existing program such as ANSYS CFX is arguably more accessible for working professionals and less time consuming compared to the creation of a new numerical model.

In the design of any floating or fixed marine structure, it is vital to test models in order to understand the fluid/structure interaction involved. Inevitably, laboratory experiments will be carried out in a wave tank or wave basin, followed by tests as in real sea conditions. However, with the developments in computational fluid dynamics (CFD) software, it is

now possible to carry out inexpensive and relatively quick initial studies. That is, provided that the numerical model used is a representative of the real life environment.

The numerical models used to model wave-tanks are known as numerical wave tanks (NWT's). NWT's are developed using a variety of numerical techniques, including the boundary volume method (BVM), the finite element method (FEM) and the finite difference method. In a NWT, a wave is generated at the input boundary and damped out near the output boundary.

Kim, et al. (2001) [16] and Park, et al. (2004) [17] numerically simulated 3D nonlinear multi-directional waves using a finite difference method. The waves were generated using a numerical wavemaker by specifying the water particle velocities at the wavemaker boundary. Koo and Kim (2004) [18] expanded the process to fluid-structure interaction in order to explore the effects of a nonlinear wave on a freely floating body for the 2D case. Sun and Faltinsen (2006) [19] developed a 2D numerical tank using the boundary element method in order to simulate the impact of a horizontal cylinder on the free surface. Ning and Teng (2007) [20] used a three-dimensional higher order boundary element model to simulate a fully nonlinear irregular wave tank. Ning, et al. (2008) [21] expanded this study to infinite water depth for nonlinear regular and focused waves. On the other hand, Yan and Liu (2011) [22] developed a 3D numerical wave tank using a high-order boundary element method (HOBEM) in order to simulate nonlinear wave-wave and wave-body interactions. The fluid motion inside a sphere was an example of wave-body interaction that they explored.

Wu and Hu (2004) [23] used a FEM numerical tank with a wavemaker to simulate the nonlinear interaction between water waves and a floating cylinder. Hadzic, et al. (2005) [24] created a 2D NWT using a commercial CFD software package to explore the motion of a floating rigid body with up to 6 degrees of freedom as it is subjected to large amplitude waves. Turnbull, et al. (2003) [25] investigated the effects of inviscid gravity waves on a submerged fixed horizontal cylinder in a 2-D FEM numerical wave tank.

Agamloh, et al. (2008) [26] used a commercial CFD software package to develop a 3D numerical wave tank, which allowed fluid-structure interaction of a water wave and a cylindrical ocean wave energy device to be explored. Both the response of a single device

and the response of an array of devices were investigated. Sriram, et al. (2006) [27] used a piston type wavemaker to generate 2D nonlinear waves using FEM. Sriram et al. (2006) [27] used a cubic spline approximation with the finite element approach when discretising the domain and had a fully reflecting wall at the end of the boundary. Contento (2000) [28] used a 2D numerical wave tank, which was based on the BEM technique, to simulate the nonlinear motions of arbitrary shaped bodies in order to develop improved seakeeping techniques. Mousaviraad et al. (2010) [29] developed a harmonic group single run sea keeping procedure, which was solved using a general purpose unsteady Reynolds averaged Navier–Stokes (RANS) solver. A linear potential solution was specified at the input boundary in order to generate linear input waves. Liang et al. (2010) [30] also explored the use of a piston type wavemaker to generate an irregular wave train using FEM. In 2008, Lal and Elangovan (2008) [31] explored the CFD simulation of linear water waves for a flap type wavemaker using the same finite volume package described in this thesis. However, the dimension of the model was taken as an experimental wave tank and simulations were only carried out for the shallow water case.

3 CHAPTER 3: THEORITICAL BACKGROUND

3.1 Computational Fluid Dynamics (CFD)

Computational fluid dynamics has certainly come of age in industrial applications and academia research. In the beginning, this popular field of study was primarily limited to high-technology engineering areas of aeronautics and astronautics, but now it is a widely adopted methodology for solving complex problems in many modern engineering fields. CFD, derived from different disciplines of fluid mechanics and heat transfer, is also finding its way into other important uncharted areas especially in process, chemical, civil, and environmental engineering. Construction of new and better-improved system designs and optimization carried out on existing equipment through computational simulations are resulting in enhanced efficiency and lower operating costs[15].

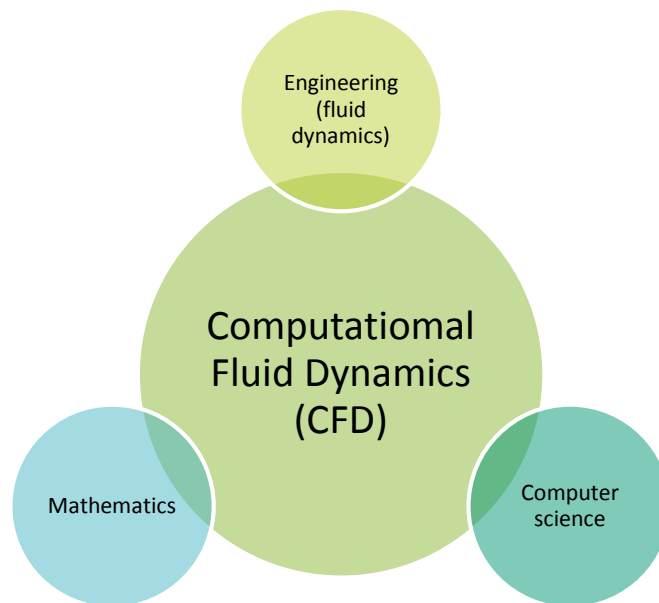


Figure 3.1 The different disciplines contained within computational fluid dynamics

In reconsideration, it has certainly become a new branch integrating not only the disciplines of fluid mechanics with mathematics but also with computer science as illustrated in Figure 3.1. Fluid mechanics is essentially the study of fluids either in motion or at rest. CFD is particularly dedicated to the former, fluids that are in motion, and how the fluid flow behavior influences processes that may include heat transfer and possibly chemical reactions in combusting flows. This directly infers to the fluid dynamics

description appearing in the terminology. Additionally, the physical characteristics of the fluid motion can usually be described through fundamental mathematical equations, usually in partial differential form, which govern a process of interest and are often called governing equations in CFD. In order to solve these mathematical equations, they are converted by computer scientists using high-level computer programming languages into computer programs or software packages.

The computational part simply means the study of the fluid flow through numerical simulations, which involves employing computer programs or software packages performed on high-speed digital computers to attain the numerical solutions[32].

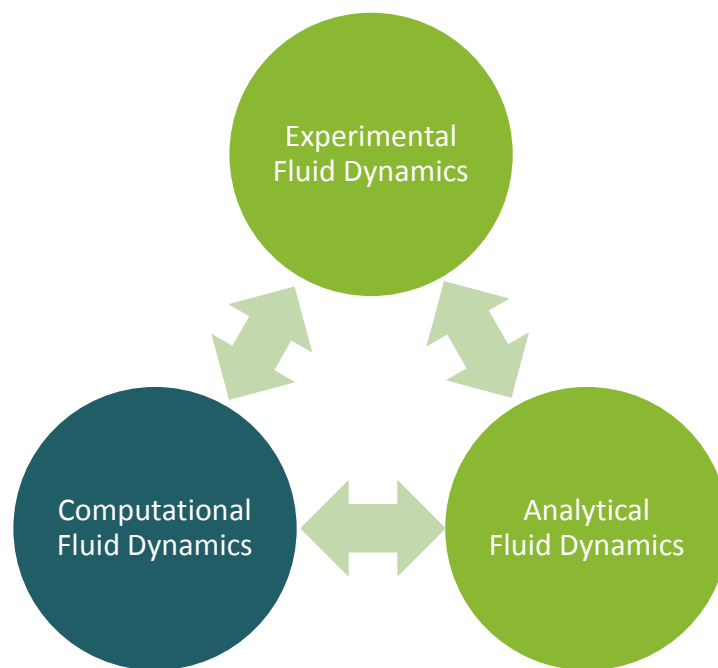


Figure 3.2 The three basic approaches to solve problems in fluid dynamics

CFD has also become one of the three basic methods or approaches that can be employed to solve problems in fluid dynamics and heat transfer. As demonstrated in Figure 3.2, each approach is strongly interlinked and does not lie in isolation. Traditionally, both experimental and analytical methods have been used to study the various aspects of fluid dynamics and to assist engineers in the design of equipment and industrial processes involving fluid flow and heat transfer. With the advent of digital computers, the computational (numerical) aspect has emerged as another viable approach. Although the analytical method is still practiced by many and experiments will continue to be

significantly performed, the trend is clearly toward greater reliance on the computational approach for industrial designs, particularly when the fluid flows are very complex[33].

3.2 CFD Theory

The fundamental equations used are the Navier-Stokes equations for an incompressible [15, 34, 35] [36, 37], constant viscosity fluid based on the three laws of conservation, which are:

1. Conservation of Mass based on continuity.
2. Conservation of Momentum based on Newton's second law.
3. Conservation of Energy based on the first law of thermodynamics.

3.2.1 Conservation of mass

The continuity equation (3.1) states that the mass is constant in a given system. Meaning that the amount of mass into the system is equal to the mass out of the system. In (3.1) \mathbb{V} represents the volume, ρ the density, m the mass, and t the time. By rewriting the total derivative, given in equation (3.2), and relate the rate of volume change to the normal-strain rate and further to the fluid velocity we get the more known continuity equation given in equation (3.3). In a numerical wave tank, the fluid can be assumed incompressible, with constant density, and the continuity equation reduces to equation (3.4).

$$\frac{Dm}{Dt} = \frac{D(\rho\mathbb{V})}{Dt} = 0 \quad (3.1)$$

$$\frac{D}{Dt} = \frac{\partial}{\partial t} + (\mathbf{V} \cdot \nabla) = 0 \quad (3.2)$$

$$\frac{\partial \rho}{\partial t} + \nabla(\rho\mathbf{V}) = \mathbf{0} \quad (3.3)$$

$$\nabla(\mathbf{V}) = 0 \quad (3.4)$$

Where the Del operator is defined in Cartesian coordinates by

$$\nabla \equiv \frac{\partial}{\partial x} \mathbf{i} + \frac{\partial}{\partial y} \mathbf{j} + \frac{\partial}{\partial z} \mathbf{k}$$

In addition, the fluid velocity vector is

$$\mathbf{V} = u\mathbf{i} + v\mathbf{j} + w\mathbf{k}$$

Where u, v and w are the velocity components, \mathbf{i} , \mathbf{j} and \mathbf{k} are the unit vector in the direction of the Cartesian coordinates x,y and z respectively.

3.2.2 Conservation of momentum

The conservation of momentum are often referred to as the Navier Stokes equation in fluid mechanics. From Newton's second law, the total force is given as the rate of change of momentum. Momentum is often noted as mass times velocity, as shown in equation (3.5) with constant mass m outside of the total derivative. In a given system the conservation of momentum means that the momentum into the system equals the momentum out of the system. In practice, this illustrates Newton's third law between fluid particles were an equal and opposite force will act on each particle in order to conserve the momentum. By dividing the mass of the fluid particle with its volume, the mass can be represented only with density, ρ . Further, the sum of forces per volume can be divided into a body force and surface forces from external stresses as given in the stress-strain formulation of Navier Stokes in equation (3.6)

$$\sum F = m\mathbf{a} = m \frac{D\mathbf{V}}{Dt} = \rho V \frac{D\mathbf{V}}{Dt} \quad (3.5)$$

$$\rho \frac{D\mathbf{V}}{Dt} = \mathbf{f} + \nabla \cdot \sigma \quad (3.6)$$

The body force, \mathbf{f} given in equation (3.7), represents the forces which is applied to the total mass of the fluid element, usually given as the gravity force per unit volume ρg . In a numerical wave tank, the buoyancy force must also be taken into consideration together with the gravity force. A buoyancy force is in general a force due to difference in density. We have assumed constant density but due to the two-phase flow between water and air in a wave tank, we have to take the difference between the fluids into account.

In CFX solver manual, ANSYS (2013), the buoyancy term is given as $(\rho - \rho_{ref})\mathbf{g}$ and will replace the hydrostatic pressure gradient given as the gravity force per unit volume.

$$\mathbf{f} = (\rho - \rho_{ref})\mathbf{g} \quad (3.7)$$

Where the reference density ρ_{ref} is given as the density of air, ρ_{air} , with a reference location in the air phase well above the wave height.

The surface forces can be related to the velocity by the stress-strain relationship for a Newtonian fluid given in equation (3.8) with tensor notation.

$$\sigma_{ij} = -p\delta_{ij} + \mu \left(\frac{\partial u_i}{\partial x_j} + \frac{\partial u_j}{\partial x_i} \right) + \delta_{ij}\lambda\nabla(\mathbf{V}) \quad (3.8)$$

$$\delta_{ij} = \begin{cases} 0 & \text{if } i \neq j \\ 1 & \text{if } i = j \end{cases} \quad (3.9)$$

$$\sigma = - \begin{pmatrix} p & 0 & 0 \\ 0 & p & 0 \\ 0 & 0 & p \end{pmatrix} + \mu \begin{pmatrix} 2\frac{\partial u}{\partial x} & \frac{\partial u}{\partial y} + \frac{\partial v}{\partial x} & \frac{\partial u}{\partial z} + \frac{\partial w}{\partial x} \\ \frac{\partial v}{\partial x} + \frac{\partial u}{\partial y} & 2\frac{\partial v}{\partial y} & \frac{\partial v}{\partial z} + \frac{\partial w}{\partial y} \\ \frac{\partial w}{\partial x} + \frac{\partial u}{\partial z} & \frac{\partial w}{\partial y} + \frac{\partial v}{\partial z} & 2\frac{\partial w}{\partial z} \end{pmatrix} \quad (3.10)$$

Where δ is the Kronecker delta function, equation (3.9) and λ the bulk viscosity which will disappear due to the incompressible assumption. The pressure is due to the fact that when the fluid is at rest the viscous stresses vanish and we are left with the hydrostatic pressure normal to the surface. The expanded form of the stress-strain relationship is given in equation (3.10).

With constant viscosity and density, the Navier Stokes equation can be written as in equation (3.11). The shear stress term $\nabla \cdot \sigma$ becomes $\mu\nabla^2\mathbf{V}$,

$$\rho \frac{D\mathbf{V}}{Dt} = (\rho - \rho_{ref})\mathbf{g} - \nabla p + \mu\nabla^2\mathbf{V} \quad (3.11)$$

Where ∇^2 is the vector Laplacian.

3.2.3 Conservation of energy

The conservation of energy, given in equation (3.12), states that heat added and work done on the system will increase the total energy of the system. Refer to Tu et al. (2008)[15] for more details. The temperature is of minor importance in a numerical wave tank with isothermal conditions.

$$\rho \frac{Dh}{Dt} = \frac{D\rho}{Dt} \nabla(k\nabla T) + \Phi \quad (3.12)$$

Where h is the enthalpy, k is the thermal conductivity and Φ is the dissipation function.

From the three equations, continuity, momentum and energy conservation, the three unknowns; pressure, velocity and temperature can be found. These parameters are the main output parameters in a CFD analysis and are the basis for all the other results.

3.2.4 Discretization using ANSYS CFX

The discretization used in ANSYS CFX is based on a Finite-Volume Method (FVM). The discretized finite volumes is constructed from the modeled mesh and in each finite volume the mass, momentum and energy is conserved. The method is always three dimensional due to the finite volumes. A two dimensional analysis can be done by only using one element in the extruded third direction. The conservation equations are further integrated over each control volume. Volume integrals of divergence and gradient operators are converted to surface integrals by Gauss' Divergence Theorem. The conservation is exactly satisfied in each control volume, which indicate also exactly conservation of the total domain. The volume and surface integrals are further discretized in order to be solved numerically. For the advection terms, the discretization used in ANSYS CFX is given in equation (3.13). [38]

$$\phi_i = \phi_u + \beta \Delta \phi \Delta \vec{r} \quad (3.13)$$

In equation (3.13), ϕ_u is the upwind discretized value and ϕ_i is the discretized value at the integration node. \vec{r} is the vector from the upwind node to the integration node. β is the blend factor which is between 0 and 1. When $\beta = 0$ a pure upwind scheme is obtained, which is robust but can introduce diffusive discretization errors. The high resolution scheme use a variable β value chosen as high as possible. When $\beta = 1$ a second order

accuracy in space is achieved. In the present work a high resolution scheme and a specified blend of $\beta = 1$ has been used.

Regarding the time discretization, a second order Backward Euler discretization scheme has been used and is given in equation (3.14)

$$\frac{\partial}{\partial t} \int_{\mathbb{V}} \rho \phi d\mathbb{V} \approx \mathbb{V} \frac{1}{\Delta t} \left(\frac{2}{3} (\rho \phi) - 2(\rho \phi)^o + \frac{1}{2} (\rho \phi)^{oo} \right) \quad (3.14)$$

In equation (3.14), the super script “o” and “oo” indicate previous iteration and the one before, \mathbb{V} is the volume, ρ is the density and ϕ is the discretization value. The second order Backward Euler Method is robust, implicit, and conservative in time and have no time step limitation. The equation is not bounded and can give nonphysical oscillations. Refer to the user manual of ANSYS (2013) for further information regarding the discretization schemes.[38]

3.2.5 Turbulence models

In a wave tank with only non-breaking regular waves the flow will follow the orbital motion and can be assumed laminar, in similar manner as if a uniform current flow will be laminar. If no structure is disturbing the fluid flow, no separation and turbulent mixing will occur. In a real water of fluid, the flow around structures will in most cases be turbulent and a turbulence model must be set up. From Reynolds decomposition, the velocity can be written as a mean velocity and a fluctuation velocity as in equation (3.15) and Figure 3.3 [33].

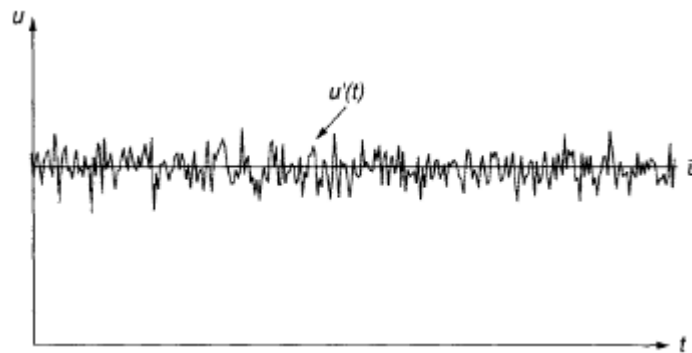


Figure 3.3 Velocity fluctuating with time at some point in a turbulent flow [15]

By adding a fluctuation velocity in all three directions and insert, it into the Navier-Stokes equations we get the Reynolds Averaged Navier Stokes (RANS) equations given in equation (3.16).

$$\mathbf{u} = \bar{\mathbf{u}} + \mathbf{u}' \quad (3.15)$$

$$\rho \frac{D\bar{\mathbf{v}}}{Dt} = (\rho - \rho_{ref})\mathbf{g} - \nabla \bar{p} + \nabla \left(\mu \left(\frac{\partial u_i}{\partial x_j} + \frac{\partial u_j}{\partial x_i} \right) - \rho \overline{u'_i u'_j} \right) \quad (3.16)$$

The last term in equation (3.16), $-\rho \overline{u'_i u'_j}$ is the apparent turbulent stresses which are unknown. The system will now have more unknowns than equations. A turbulence model will give the relation between the extra-unknown turbulent stresses and the mean flow variables. All turbulence models have some empirical relations and the choice of model will depend upon the problem to solve. The turbulence models can be divided into Eddy viscosity models, Reynolds stress models and Eddy simulation models. The eddy viscosity models use the Boussinesq hypothesis by using an eddy (or turbulence) viscosity, μ_t . The Reynolds stress models use transport equations for the Reynolds stresses and the Eddy simulation models (LES and DES) resolves the eddies without the RANS formulation. The most used models among engineers are the Eddy viscosity models and especially the $K - \epsilon$ model. In the present work, a $K - \epsilon$, and a SST (Shear Stress Transport) model has been used.[15]

3.2.5.1 Eddy viscosity models

The Boussinesq hypothesis, referred from Andersson (1988)[39], links turbulent, or Reynolds stresses to the mean rate of deformation as shown in equation (3.17). This only moves the turbulent unknown from the apparent stresses to a turbulent viscosity, μ_t . The model is a two-equation model, which relates the unknown turbulent viscosity, μ_t to the turbulent kinetic energy, K , and the turbulent dissipation ϵ . The relation is given in equation (3.18).

$$\rho \overline{u'_i u'_j} = \mu_T \left(\frac{\partial u_i}{\partial x_j} + \frac{\partial u_j}{\partial x_i} \right) \quad (3.17)$$

$$\mu_T = \rho C_\mu \frac{K^2}{\epsilon} \quad (3.18)$$

Here $C_\mu = 0.09$ for the model. Near walls, the model use a wall function. A scalable wall function uses the logarithmic velocity profile approximated from the velocity close to the wall. The boundary layer can be divided into a sub layer with almost linear velocity profile, a logarithmic layer following the logarithmic profile and a buffer layer where the laminar and turbulence effects are of equal importance. A boundary layer is shown in Figure 3.4.

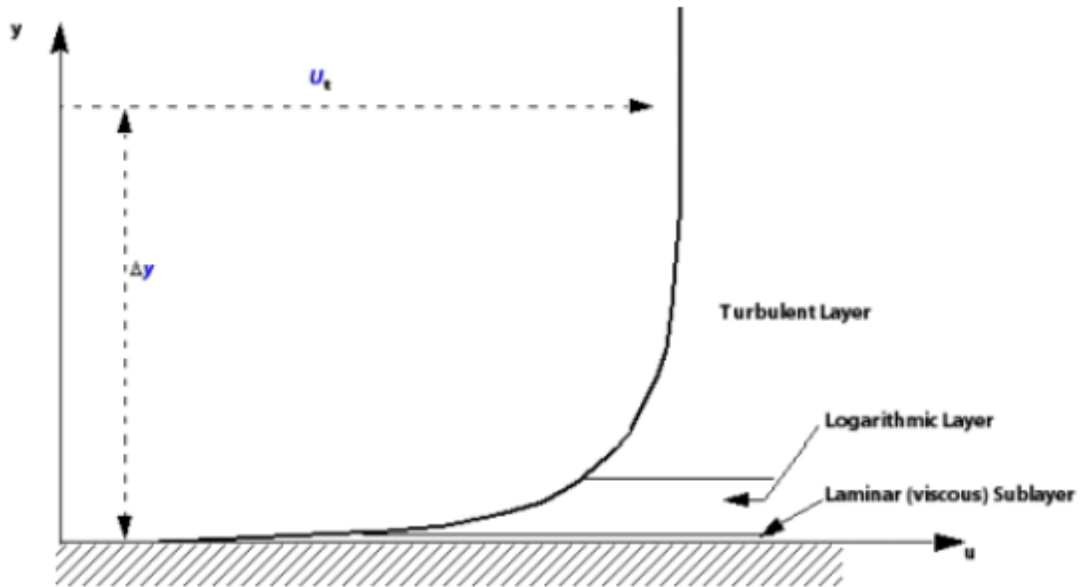


Figure 3.4 Boundary layer showing the sub layer, logarithmic layer and the buffer layer. ANSYS (2013).

The logarithmic profile is often mentioned as the "log law of the wall". One important issue with a wall function is the lack of modeling separation in the boundary layer. When the flow separates, the velocity gradient becomes zero at the wall and the velocity profile will turn over and become negative. A wall function based on the logarithmic profile will not be able to represent a zero velocity gradient or back flow. In waves, the velocity profile oscillates with the wave period and follow the orbital motions with reduced radius

towards the bottom. A wall function without capability of separation should therefore not be used overall in a numerical wave tank.

The SST (Shear Stress Transport) model of Menter (1994) [40] is based on the two-equation K- ω model. Menter (1994) is the head of the turbulence program of ANSYS CFX. Here K still is the turbulent kinetic energy and ω is the turbulent frequency. Similar to the K- ω model the SST model gives a more accurate flow near walls with an automatic switch from a wall function to a low-Reynolds number method. For the low-Reynolds number method the mesh close to the walls is assumed fine enough to resolve the viscous part of the boundary layer. The SST model use in this way the best from both the SST model and the K - ω model with use of the K - ω model for near wall treatment and the model in the bulk flow. The SST model can therefore be used when the boundary layer does not follows the logarithmic profile given in a wall function as long as the mesh is fine enough to resolve the turbulence. In equation (3.19), the turbulent viscosity is given for the SST model.

$$\mu_T = \rho \left(\frac{a_1 k}{\max(a_1 \omega, S F_2)} \right) \quad (3.19)$$

Where $a_1 = 5/9$, S is the invariant measure of the strain rate and F2 is a blending function given in (3.20).

$$F_2 = \tanh \left(\left(\max \left(\frac{2\sqrt{k}}{\beta^* \omega y}, \frac{500\nu}{y^2 \omega} \right) \right)^2 \right) \quad (3.20)$$

In a CFD analysis, the characteristics of the chosen turbulence model must be specified. There are several alternatives. The turbulent kinetic energy K and the turbulent dissipation ϵ or the turbulent frequency ω can be specified. Alternatively, a length scale or an eddy viscosity ratio can be specified instead of the ϵ or ω value. A third alternative is to specify the intensity of the turbulence instead of the kinetic energy. The intensity is given as the ratio between the turbulent fluctuation velocity and the mean velocity. In the present work, medium turbulence is used when a turbulence model is selected. Medium intensity is given as 5% intensity and an eddy viscosity ratio equal 10. Medium turbulence is the recommended setting if you have no information regarding the turbulence[33].

3.2.6 Free surface

The first necessary condition to fulfill in order to model a numerical wave tank is the capability of modeling a free surface flow. Free surface flows are in general a special case of multiphase flows with one liquid and one gas phase, respectively water and air in this case. Also mentioned as a two-phase flow. The free surface can be noted as a boundary, which split the two phases. One of the major issue is that the free surface boundary are not rigid, but it is dynamically free. The actual position of the surface is only known at the initial time and will be part of the solution for later time steps. In order to be able to find the free surface position as function of both time and space, boundary conditions is necessary.

Free Surface Boundary Conditions

There exists two conditions defining the free surface:

1. Kinematic boundary condition
2. Dynamic boundary condition

The *kinematic boundary condition* requires that the water particles at the free surface stay at the free surface. This indicates no net fluid flow through the free surface. The normal water velocity component located at the free surface has to be equal to the normal velocity component of the free surface boundary, equation (3.21).

$$[(v - v_b)\mathbf{n}]_{f_s} = 0 \quad \dot{m}_{f_s} = 0 \quad (3.21)$$

Here v is the water velocity, v_b the boundary velocity, \dot{m}_{f_s} the mass flux and f_s indicates the free surface. The *dynamic boundary condition* requires force equilibrium at the free surface. Normal forces on the surface has to be equal and opposite in direction and tangential forces equal and in the same direction. In gravity driven free surface flows, the surface tension force and the viscous shear stress force at the surface can be neglected, and we are left only with the pressure force. This gives water pressure equal to the air pressure at the free surface, equation (3.22).

$$[p_{water} - p_{air}]_{f_s} = 0 \quad (3.22)$$

Since the location of the free surface is unknown and becomes a part of the solution, one can only use one of the boundary conditions at the surface. The other boundary condition is needed to locate the surface position iteratively. There are several methods to define the surface position, and they can be classified into two main groups:

1. Interface Tracking method
2. Interface Capturing method

In the interface tracking method, the free surface is defined as a sharp interface. The mesh is shaped according to the surface boundary, which will follow the wave elevation. This requires a moving mesh, which must be regenerated for each time step. The other method, interface capturing method, is used with a fixed mesh extended into the air. The volume cells will all be specified with a volume fraction of air and water. The free surface will then be located along the volume cells with a volume fraction of 0.5, which indicates equally filled with water and air. This method is also referred to as a *Volume tracking method* since it tracks cells with equally water and air fraction. The first capturing method was the Marker and Cell method, (MAC). Later on this method developed to the *Volume of Fluid method*, (VOF) which is used by many CFD solvers.

Due to the fact that all cells would have a water and air fraction this method was time consuming earlier and the interface tracking method was preferred since it was faster. With increasing computer power, the interface capturing method has become more popular. Also for reasons that the interface capturing method is more robust and can handle effects as flow spray and breaking waves. For the interface tracking method only simple wave profiles can be studied, were the mesh cells can follow the surface boundary. This limits the method from effects as breaking waves. In Figure 3.5 volume cells with given water fraction is shown.

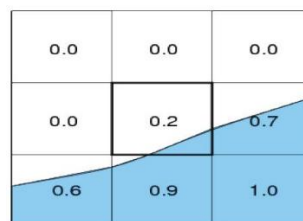


Figure 3.5 Water fraction

ANSYS CFX use the *interface capturing method* to define the free surface. To get the free surface as thin as possible the mesh must be very fine with high density in the region covering the free surface. In the practical computation, the free surface will be smoothed over some grid cells. Adaptive mesh refinement is often used for unstructured meshes in steady state analysis were cells with water fraction of 0.5 will be refined, the solver then refines the area close to the free surface automatically Figure 3.6.

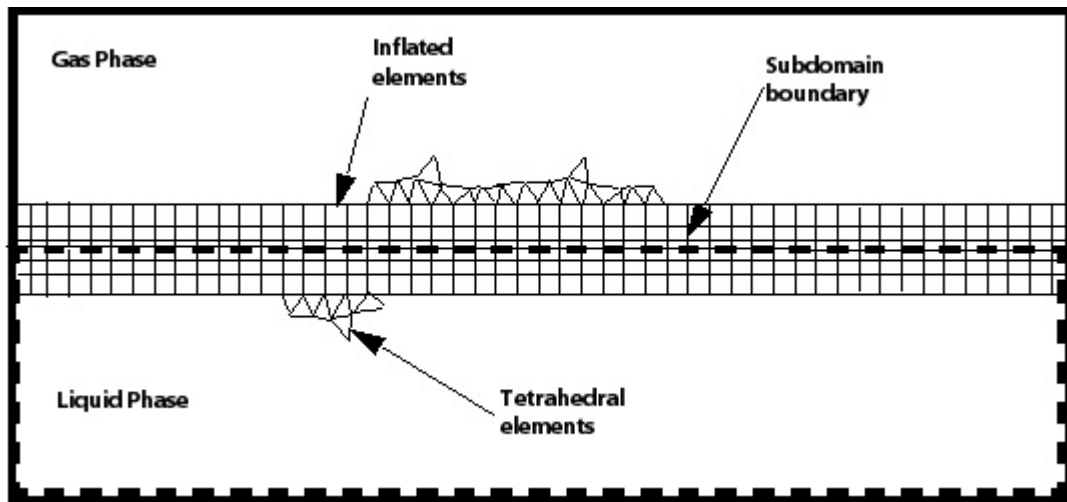


Figure 3.6 An exaggerated view of three inflation layers on each side of the uppermost subdomain boundary surface [38]

In a numerical wave tank, a transient simulation is necessary. The mesh around the free surface are therefore refined uniformly around the initial location of the free surface.

3.2.7 Overview of domain boundary conditions

In a CFD analysis, the problem to solve is bounded and modeled by a domain. The domain boundaries has to be specified in order to have a solution. The most used boundary conditions in a numerical wave tank are shortly listed in the following. Refer to the specific section for more information regarding the actual boundary conditions used in each analysis. Further details can also be found in the user manual of ANSYS (2013).

3.2.7.1 Inlet boundary condition

At an inlet boundary condition all fluid quantities has to be specified. At the boundary the velocity components can be specified in all three directions, the mass flow rate can be specified or the pressure can be specified. From the specified values, the convective fluxes

can be directly calculated. The gradient driven diffusive fluxes can be found from an approximation of the gradients. If the fluid conditions at the inlet not is known, the inlet should be placed far from the studied part of the domain. In addition to the fluid specifications, the turbulence settings must be specified at the inlet.

3.2.7.2 Outlet boundary condition

Similar to the inlet condition, the outlet should be placed far away from the studied part of the domain since normally little information is known at the outlet. Most used outlet condition is to specify the pressure since the velocity profile usually not is known. In a numerical wave tank a static pressure can be used which will give a constant mean free surface level at the outlet. The static pressure condition is crucial to the dynamic wave elevation; it will force the elevation to the mean surface level at the outlet. If the wave elevation could be prescribed at the outlet, a dynamic pressure condition could be used.

3.2.7.3 Opening

An opening boundary condition allows the fluid to flow both ways through the boundary. Here pressure with direction, velocity or entrainment can be specified. The entrainment option can be useful in situations where the flow direction is unknown. The turbulence settings also need to be specified. In flows where the flow oscillates or the fluid is free to move in or out, an opening boundary is often used.

3.2.7.4 No slip and free slip wall

An impermeable wall is a physical boundary, which limits the fluid to flow through. The physical condition states that $U_i = U_{i,wall}$, indicating similar tangential fluid velocity on the wall as the wall velocity. The normal velocity on the wall is set to zero. With no fluid flow through the wall, the convective fluxes can be set to zero. If the wall is fixed, also the tangential velocity on the wall is zero, indicating the no slip condition. A moving wall can also have a no slip condition if the fluid has the same tangential velocity as the wall. In a piston or flap type wave maker an impermeable moving wall will force the fluid into motion. For a free slip wall the tangential fluid velocity are not affected by the wall and only the normal velocity on the wall is set to zero, $U_{n,wall} = 0$. On a free slip wall also the wall shear stress is set to zero, $\tau_w = 0$. In connection with turbulence, the roughness can be specified. A wall can also be used as a thermal boundary with heat convection.

3.2.7.5 Symmetry plane

In steady flows symmetric solutions can be obtained. If the geometry and the flow field is assumed to be symmetric, a symmetry plane can be used. By only solving half the domain and introduce a symmetry plane in order to get the total solution, computation time can be reduced. On the symmetry plane all the convective fluxes is set to zero. The normal velocity is set to zero, but the velocity gradients normal to the plane can be non-zero indicating that the normal stress is non zero. The tangential velocity on the symmetry plane can be non-zero, but the normal gradients of the parallel, or tangential, velocity components are zero. The boundary condition requires no input. In a numerical wave tank, the tank walls can be set as symmetry condition in order to perform a 2D analysis.

3.2.7.6 Domain Interface

Between sub domains, a connection interface condition has to be set up. A common interface connection is the General Grid Interface (GGI) condition, which connect two different regions to each other. The GGI connection is an implicit and conservative connection which also can be used in cases where the grid on both sides does not match. A balance of the mass and momentum fluxes is achieved by evaluating the fluxes on each side of the interface.

3.3 Potential Wave Theory

The wave theory used in the present work is based on the potential theory. In the potential theory three well known assumptions can be summarized as follows:

1. Incompressible: $\frac{\partial \rho}{\partial x} = 0$
2. Inviscid: $\nu = 0$
3. Irrotational: $\nabla \times \vec{v} = 0$

Where ρ is the density, ν is the kinematic viscosity, ∇ is the Del operator, and \vec{v} is velocity vector.

The incompressible assumption states that the density, ρ is constant. In an inviscid fluid the viscosity is equal zero. Irrotational flow means that the curl of the velocity is zero, or in other words, the local angular velocity in a given point is zero. By these assumptions

together with the given boundary conditions, a velocity potential for regular waves can be expressed.

A linear velocity potential is given in equation (3.23) valid for all water depths with linear assumptions for the wave parameters. The surface elevation for this potential is given in equation (3.24).

$$\phi = \frac{Hg \cosh k(h+z)}{2\omega \cosh kh} \cos kx \sin \omega t \quad (3.23)$$

$$\eta = \frac{H}{2} \cos(kx - \omega t) \quad (3.24)$$

From the derivatives of the velocity potential, the wave velocities can be expressed, given in equation (3.25) and (3.26).

$$u = -\frac{\partial \phi}{\partial x} = \frac{H}{2} \omega \frac{\cosh k(h+z)}{\sinh kh} \sin(kx - \omega t) \quad (3.25)$$

$$w = -\frac{\partial \phi}{\partial z} = \frac{H}{2} \omega \frac{\sinh k(h+z)}{\sinh kh} \cos(kx - \omega t) \quad (3.26)$$

The linear surface elevation and velocities will be used as input in the first modeled method of a numerical wave tank. In the theoretical approach, the linear dynamic pressure will be integrated to find pressure forces. The surface elevation and velocities will also be used in comparison with numerical and experimental results, see Figure 3.7.

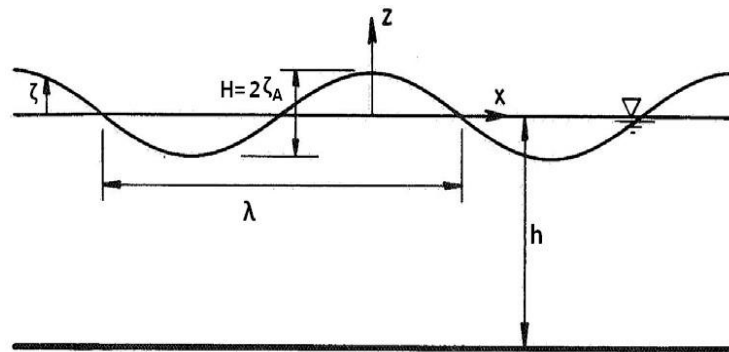


Figure 3.7 Wave characteristics [41]

3.4 Breaking Wave

Another criterion, which limits the waves, is the breaking criterion. If the wave steepness, $S = \frac{H}{\lambda}$ becomes too large the wave will break Figure 3.8. The wave theory will therefore not be valid with wave parameters when braking waves will occur. The critical value for the wave steepness is given as $S_{crit} = 1/7$ for regular waves in deep water. When the wave height become higher than $1/7$ wavelength in deep water the wave will break. In an arbitrary water depth, the breaking criteria can be found by the Miche criterion given in equation (3.27), Miche (1951)[42].

$$\frac{H}{\lambda} = \frac{1}{7} \tanh \left(5.5 \frac{h}{\lambda} \right) \quad (3.27)$$

In deep water, h becomes large and equation (3.27) gives the deep water steepness criteria. In shallow water when the water depth is small compared to the wavelength $\tanh \left(5.5 \frac{h}{\lambda} \right) \approx 5.5 \left(\frac{h}{\lambda} \right)$ and the criteria becomes $H_{crit} = 0.78h$ (based on solitary wave theory).

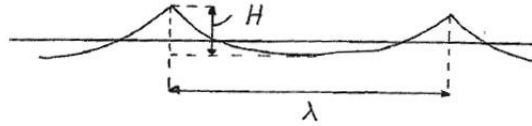


Figure 3.8 Definition of wave height and wave length

3.5 Wavemaker Theory

In all laboratory experiments with water waves, the wavemaker is important to produce the wanted waves. The production of waves can be done by many different methods and are in fact a common result from any moving object in a free surface fluid. In the wavemaker theory, a relation between the free surface motion and the wavemaker object must be set up to produce the wanted waves. One of the easiest ways to produce waves is to move a piston, or a wall, normal to the free surface periodically. Dean and Dalrymple (2000) [41] give a brief overview of the wavemaker theory for a piston and a flap. In Figure 3.9 a simplified shallow water piston-type wavemaker theory is shown.

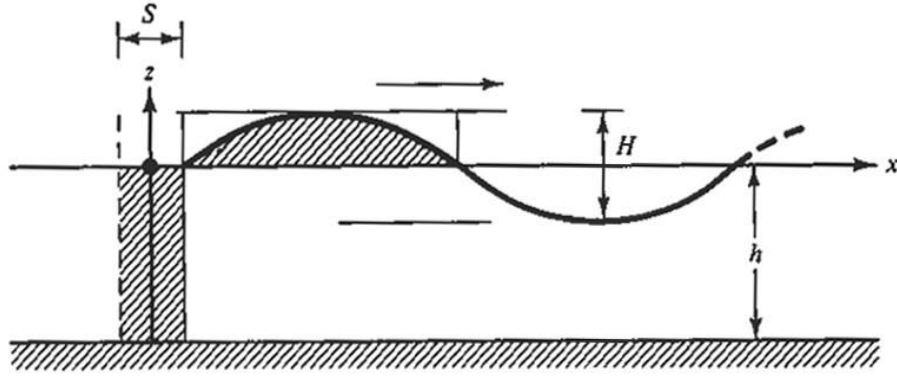


Figure 3.9 Simplified shallow water piston-type wavemaker theory of Galvin [41]

The principle is to relate the volume of water displaced by the piston over a whole stroke to the volume of water under a wave crest. The result from the water conservation given for simplified shallow water wave theory gives the relation in equation (3.28). For a bottom hinged flap the result becomes as given in equation (3.29). In equation (3.28) and (3.29) $H = 2\zeta_A$ is the wave height, $S = 2S_A$ the piston stroke, $k = 2\pi/\lambda$ is the wave number and h the water depth.

$$\left(\frac{H}{S}\right)_{piston} = kh \quad (3.28)$$

$$\left(\frac{H}{S}\right)_{flap} = \frac{kh}{2} \quad (3.29)$$

The complete wavemaker theory is deduced from the same boundary value problem for two-dimensional waves in potential theory. The kinematic and dynamic boundary conditions for the free surface and the no-slip condition for the bottom boundary are similar. The only difference is the lateral conditions, which must consider the piston, or flap motion. The horizontal displacement is given in equation (3.30) and the stroke is given in equation (3.31) with z positive upwards and origin at the free surface. If the water depth is larger than the hinged flap the stroke motion of the flap will only be valid above the hinged point, with no motion below[43].

$$x = \frac{S(z)}{2} \sin \omega t \quad (3.30)$$

$$S(z) = \begin{cases} S_{Piston} \\ S \left(1 + \frac{z}{h_h}\right)_{Flap} \end{cases} \quad (3.31)$$

The final equations for the Stroke motion from solving the boundary value problem derived Dean and Dalrymple (2000) [41] is given in equation (3.32) for the piston and (3.33) for the bottom-hinged flap.

$$\left(\frac{H}{S}\right)_{piston} = \frac{2(\cosh(2kh)-1)}{\sinh(2kh)+2kh} \quad (3.32)$$

$$\left(\frac{H}{S}\right)_{flap} = \frac{4 \sinh(kh)}{kh} \frac{kh \sinh(kh) - \cosh(kh) + 1}{\sinh(2kh) + 2kh} \quad (3.33)$$

In Figure 3.10 the wave height to stroke ratio, H/S is shown for relative depths. In Figure 3.10 the dotted lines represents the simplified wavemaker theory. The wavemaker theory is based on linear first order potential theory in shallow water with assumed small motions. The same limitations given for linear wave theory will limit the wavemaker theory. In laboratory wave basins, the wavemaker theory are usually used to give the transfer function used as input for the physical wavemaker system. In similar manner, the wavemaker theory can be used in a numerical wave tank to make numerical waves.

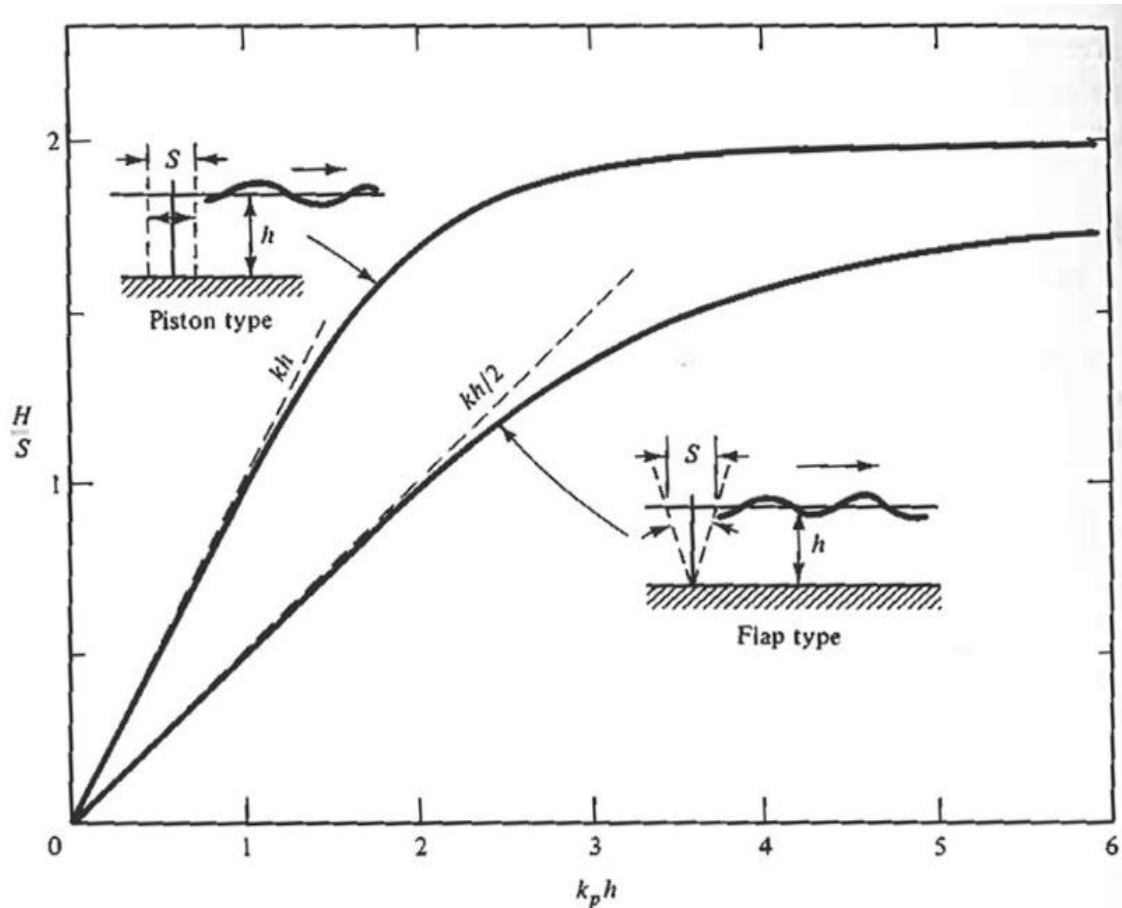


Figure 3.10 Wave height to stroke ratios versus relative depths from plane wavemaker theory [41]

3.6 Morison's Equation

Morison et al. (1950) [44] proposed the following formula for determining the total wave force, which is just the sum of the two forces, drag and inertia, Figure 3.11. Equation (3.34) shows the force per unit length.

$$F(t) = \frac{1}{2} \rho C_D A |u|u + \rho C_M \frac{\pi D^2}{4} \dot{u} \quad (3.34)$$

Where C_M is the inertial coefficient and C_D is the drag coefficient and A is the projected area perpendicular to the flow.

To determine the total force on a vertical pile, the force per unit elevation must be integrated over the immersed length pile.

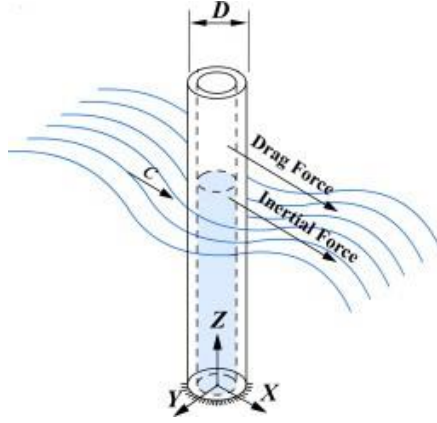


Figure 3.11 The force components of Morison equations

The total force is given in equation (3.35) using the local velocity from the linear wave theory equation

$$F = \frac{\rho C_D D H^2 g}{4 \sinh 2kh} \left(\frac{2kh + \sinh 2kh}{4} \right) \cos(kx - \omega t) |\cos(kx - \omega t)| + C_M \frac{\rho \pi D^2 H}{4k} \frac{H}{2} \omega^2 \sin(kx - \omega t) \quad (3.35)$$

Where x is the location of the pile (conveniently, this can usually be taken as $x=0$), h is the water depth, H is the amplitude of the wave, k is the wave number, and ω is the frequency of the wave.

The Total moment about the seafloor can be obtained similarly by integrating, equations (3.36) and (3.37).

$$M = \int_{-h}^{\eta} (h + z) dF \quad (3.36)$$

Which yields

$$M = \frac{\rho C_D D H^2 g}{4 \sinh 2kh} \left(\frac{2kh + \sinh 2kh}{4} \right) \cos(kx - \omega t) |\cos(kx - \omega t)| \left\{ h \left[1 - \frac{1}{2n} \left(\frac{\cosh 2kh - 1 + 2(kh)^2}{2kh \sinh 2kh} \right) \right] \right\} + C_M \frac{\rho \pi D^2 H}{4k} \frac{H}{2} \omega^2 \sin(kx - \omega t) \left\{ h \left[1 - \frac{\cosh kh - 1}{kh \sinh kh} \right] \right\} \quad (3.37)$$

Where

$$n = \frac{1}{2} \left(1 + \frac{2kh}{\sinh 2kh} \right)$$

In which each of the terms above is recognized as the total force component times the respective lever arm (the lever arms are in the braces, {, }).

4 CHAPTER 4: NUMERICAL MODEL SETUP

4.1 Numerical Wave Tank

In CFD, a domain of interest is modeled by discretized elements. In each element, a set of fundamental conservation equations is solved for each time step. The results in each element are then used as input for the next time step. From this method, a time dependent dynamic analysis can be simulated. There are today many different numerical schemes and numerical methods for fluid dynamics, both commercial software, open source codes and in house codes in the industry and at universities. For the commercial software, it is often combined with a nice interface, which makes it easier to perform analysis. For the open source and in house codes there might be more opportunities and easier to directly affect the solver equations but often not as easy to perform analysis due to limited interface. Therefore, most commercial software has been used for engineers in a time limited and profit based industry.

In connection with increased computer power and fast development in numerical fluid dynamic solvers, CFD analysis has been used in many new areas in the last years. A numerical wave tank (NWT) has been one of the new areas with increasing activity, especially for marine engineers. With a numerical wave tank, one can do almost similar analysis as many of the more expensive experiments performed in physical water basins. For many companies this will reduce both experimental costs and time performing analysis. Due to many numerical parameters involved in a numerical setup, CFD analysis usually has to be validated with experimental data. In the present time, CFD is not capable of taking over performing physical experiments. CFD analysis can instead reduce experimental test conditions and perform parameter studies. In this way physical experiments and CFD, analysis together can be a very effective tool and give faster and more accurate results [45] [46, 47].

There are today several different commercial CFD software, which are capable of wave modeling. In the present work ANSYS Workbench version 13.0 has been used to model a three dimensional numerical wave tank with ANSYS DesignModeler for geometry, ANSYS Meshing for meshing and ANSYS CFX for numerical setup and solver.

The method used to model the above cases is the piston wavemaker method. The inlet wall is given a specified oscillation motion similar to a wavemaker in a physical wave tank.

4.2 Developing the Numerical Model

CFD codes are usually structured around robust numerical algorithms, these codes (like CFX) include a user-friendly Graphical User Interface (GUI) applications and environments to input problem parameters. Therefore these codes provide a complete CFD analysis consisting of three main elements: the Pre-processor, the Solver, and the Post-processor as shown in Figure 4.1.

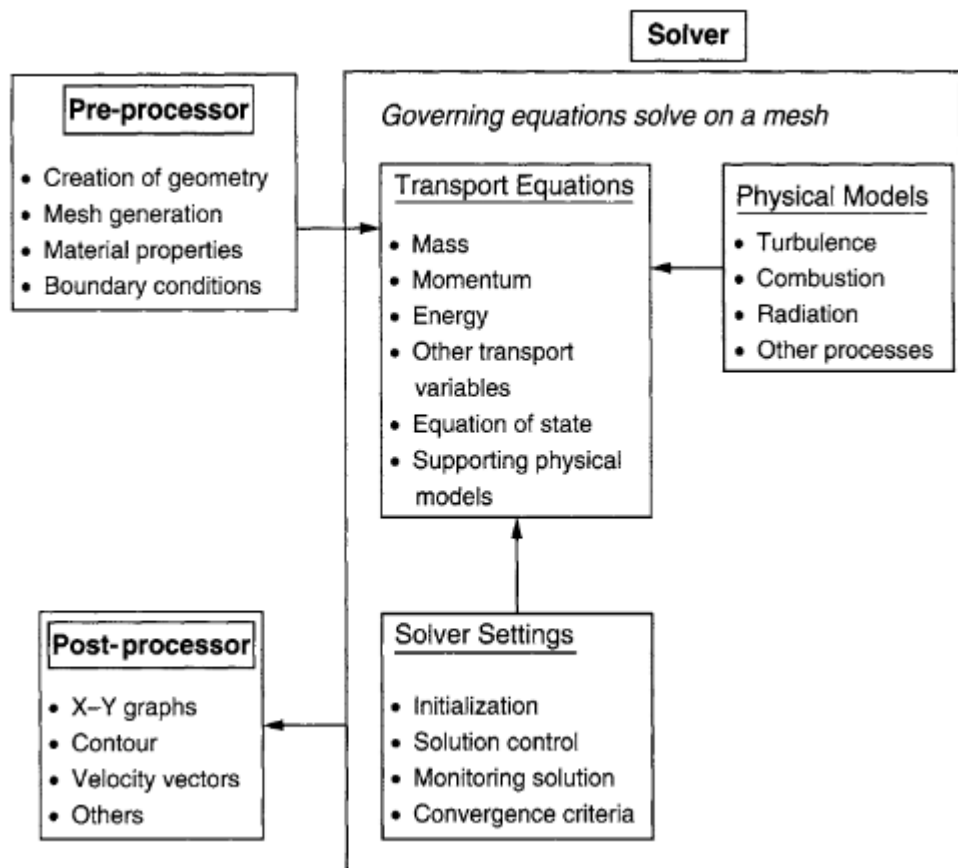


Figure 4.1 The three main elements of a CFD code

4.2.1 Domain and meshing

The CFD analysis is carried out using ANSYS Workbench. An overview of the proposed project can be seen; the necessary modules for the simulation are appered in boxes and can be linked together. The used domains have been made in ANSYS DesignModeler. A

domain was created by a set of three-dimensional blocks and then equally extruded, see Figure 4.2 [48, 49].

All the blocks were assembled into one part in order to make a continuous mesh. Further, the mesh was made in ANSYS Meshing. A sizing method was used and number of divisions was set for each side. By this method, a structural mesh was defined. In addition, named sections were made in order to link the various boundaries with boundary conditions in CFX Pre. The dimensions of the NWT, number of elements and design of the mesh are important parts since they directly influences the analysis time and solution.

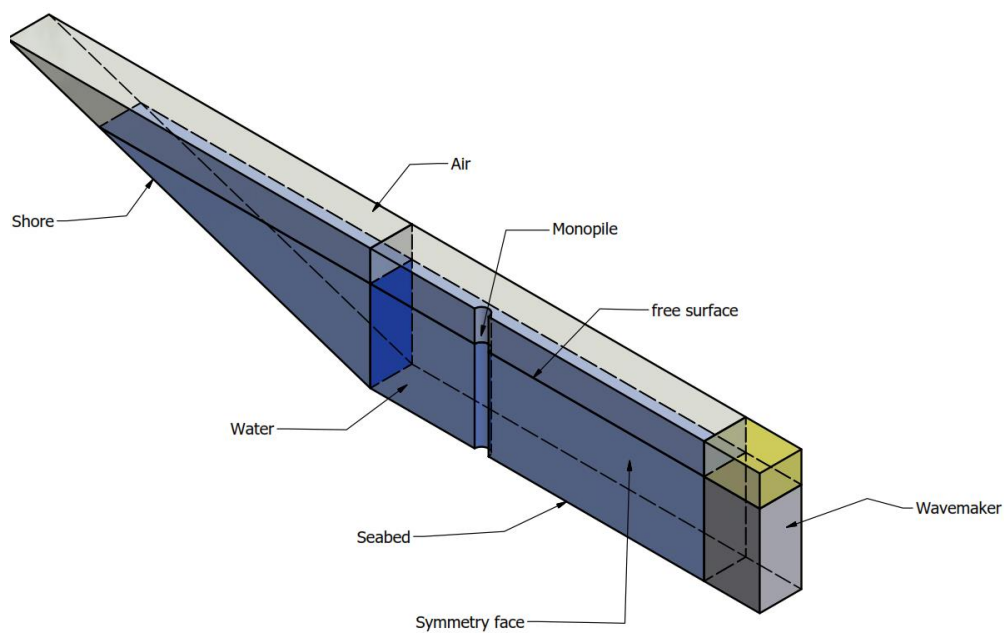


Figure 4.2 Geometry of the model

According to Finnegan and Goggins (2012)[1], the height of the model is dictated by a number of factors; the still water level, the maximum height of the waves and the response amplitude and height of the device. Therefore, since the tank is being designed for deep water wave theory, the height of the tank is estimated to be $4/3$ times the still water level, as this will leave sufficient room at the top (opening boundary) of the tank.

As it is a numerical model, the geometry of the wave tank can be easily changed. As a result, the geometry can be optimized depending on the period of the generated wave. As

the generated waves will be almost linear, linear (Airy) wave theory can be used to predict the minimum depth of the water, as follows

$$\frac{h}{L_0} > \frac{1}{2} \quad (4.1)$$

Where h is the water depth, $L_0 = gT^2/2\pi$, g is the gravity and T is the wave period.

The length of the model from the wavemaker to the beach is approximately $3h$ according to Finnegan and Goggins (2012)[1]. A beach is needed to provide damping for the wave and to avoid wave reflection, a beach with a slope of 1:3 is recommended by Silva, et al. (2010)[2].

In the article given by Finnegan and Goggins (2012) [1]it was essential to optimize the mesh size, as this will reduce computational effort. This is particularly important for 3D modeling of wave tanks. A significant observation that must be noted is the sensitivity of the wave elevation to the mesh refinement. The generated wave used in their article has a period of 1.35s, with an element size of 0.15m. Therefore Finnegan and Goggins (2012) established a simple linear relationship to estimate the minimum element size when $T = n$ seconds is given as

$$\text{Min. Element Size} = \frac{L[T=n \text{ s}]}{L[T=1.35 \text{ s}]} \times 0.15\text{m} \quad (4.2)$$

The choice of tank width depends on the proposed model tests. The most straightforward tank is a single paddle in a narrow flume that represents a 2D slice, with the model fully blocking the width of the tank. This type of model is relatively easy to analyze because the waves and flow act in a plane. Visibility is excellent and models are readily accessible. It is a very good and economic tank for early Investigations. A slightly wider tank with a Single paddle can have a 3D model subjected to long-crested waves that pass round the sides so that 3D edge effects can be observed. The main difficulty is that as the width Increases the frequency of the resonant cross wave becomes very close to the working frequency of the tank. For example a 0.7 m deep tank 1.2m wide will have a cross wave of 0.78Hz. [50]

In this thesis, the ratio between the monopile diameter to NWT width was chosen to be 0.167 as a rule of thumb, this ratio is close to the NWT of Mo et al. (2005) [5] who chosen

the ratio to be 0.14 as shown in figure Figure 4.3. Further studies of NWT width effect on total forces of the monopiles is recommended.

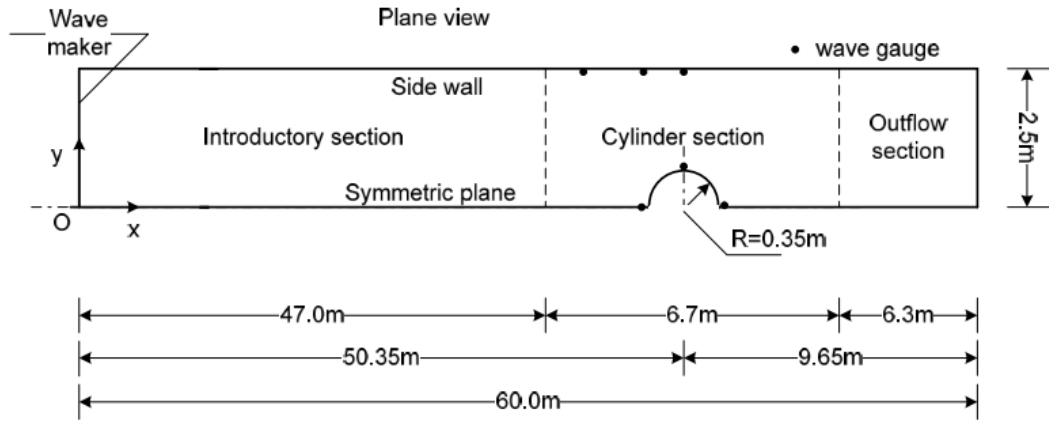


Figure 4.3 The NWT of Mo et al.[5]

4.2.2 Numerical settings

In CFX Pre, all the numerical settings are set. The domain in a numerical wave tank consist of two fluids, water and air. Density and viscosity used is given in Table 4.1.

Table 4.1 Density and viscosity of water and air

Fluid	Density ρ [kg/m ³]	Dynamic viscosity μ [kg/ms]
Water	1025	8.899×10^{-4}
Air	1.185	1.831×10^{-5}

In Table 4.1, the general numerical settings are given. In all cases, a transient analysis and a free surface model have been used. In order to have a pure 2nd order spatial discretization scheme the advection blend *General settings in ANSYS CFX* factor was set equal 1 in all cases. A smaller blend factor will give lower accuracy and a blend factor of 0 indicate 1st order upwind spatial discretization. The robustness also increase for a lower blend factor. Alternatively, the *high resolution* option can be used where the blend factor varies throughout the domain based on the local solution field. The 2nd order *Backward Euler Scheme* is an implicit time-stepping scheme recommended in general for transient runs and was used in all cases. The convergence criteria was set to a reasonable low value and number off coefficient loops was for most cases set to 2 – 6 loops in each time step.

$$AirFrac = step\left(\frac{y-h}{1.0[m]}\right) \quad (4.3)$$

$$WaterFrac = 1 - AirFrac \quad (4.4)$$

In a free surface flow, the two phases are defined by use of a volume fraction for each phase as shown in equation (4.3) and (4.4). In these equations h is the elevation of the still water level, a built in step function is used. A water volume fraction value of 1 represents water and a value of 0 represents no water. The free surface will in this way be defined at a volume fraction of 0.5. The fluid model was defined as a homogeneous multiphase model with an interface compression level of 2. A homogeneous multiphase model means that the flow field is shared for the two fluids. Only one set of momentum equations is needed since the velocity field will be identical for the two phases. The compression level sharpens the interface and gives faster convergence, but it also increase computation time. In the multiphase control, a coupled volume fraction was selected. As a comment, the homogeneous multiphase model is recommended for flows were the free surface is well defined. For flows where mixing occur, for example breaking waves, the inhomogeneous multiphase model should be used, see Table 4.2

Table 4.2 General numerical Settings

Parameter	Setting
Model	Transient
Turbulence	Laminar / $K - \epsilon / SST$
Advection Scheme	High Resolution
Time Scheme	2nd order Backward Euler
Multiphase model	Homogeneous
Interphase compression	Level 2
Volume fraction	Coupled
Mean water level	3.25m
Isothermal	Temp = 25°C

Isothermal heat transfer and buoyancy is used in all cases. The buoyancy reference density is set equal to density of air, ρ_{air} . In the solver control the advection discretization scheme, time discretization scheme, convergence criteria and number of convergence loops are set. The numerical settings are specified under each separate studied case.

Running in parallel will in many cases be suggested if available due to reduced computation time. In the present work, running in serial was selected. In the ANSYS

solver manual ANSYS (2013) the convergence issue for free surface flows in parallel is noted and some advices given.

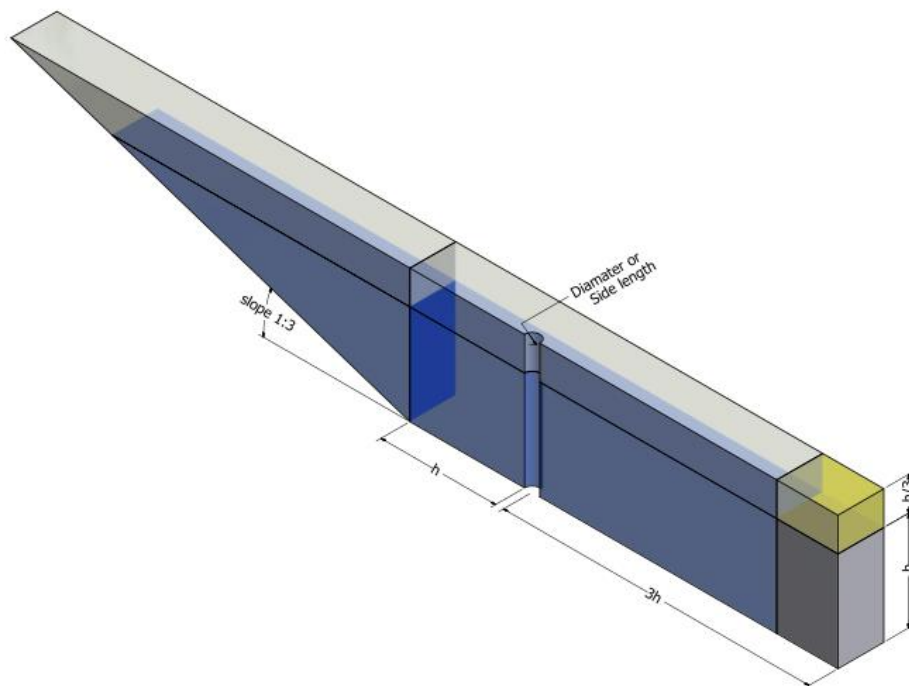


Figure 4.4 Domain dimensions

4.2.3 Producing waves at the inlet

A wavemaker can be made by several methods. In a physical wave basin, a double flap or a multi flap wavemaker is often used in order to produce both regular and irregular sea. In a numerical sense similar wavemaker as in a physical wave basin can be modeled. In, Figure 4.5 and Figure 4.6, two simple wavemakers has been compared. A piston type wavemaker, a bottom hinged flap wavemaker and a general hinged flap wavemaker. Domain size, numerical settings and mesh settings as guided by Finnegan and Goggins (2012) [1] has been used. The only difference was the dynamic motion of the wavemaker. The domain and mesh of the model is dicussed in the following sections. The domain is shown in Figure 4.4 and the general mesh parameters is given in Table 4.3. The mesh used is shown in Figure 4.7.

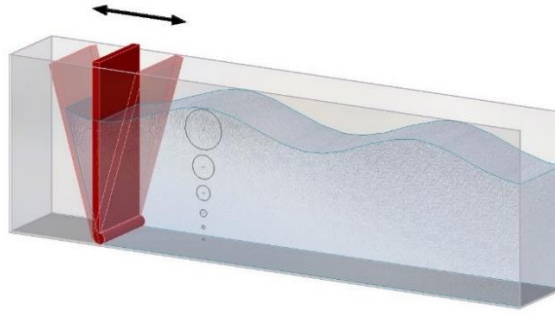


Figure 4.5 Bottom-hinged flap wavemaker

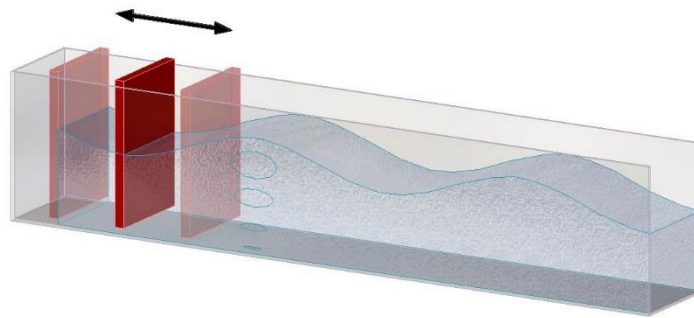


Figure 4.6 Piston wavemaker

Table 4.3 Domain and mesh properties

Parameter	Setting
Domain length	27.05m
Water depth	3.25m
Air height	1.1m
Extruded width	1.5m
Minimum mesh element size	0.25m

4.2.4 Boundary conditions and numerical settings

The domain was divided into two sub domains. The first sub domain (located in the first 2m) was set to a motion specified domain. In the motion specified sub domain, the mesh on all boundaries was set as unspecified in order to allow dynamic motion. The top, bottom, front and back boundaries was set similar for the two sub domains [5, 51].

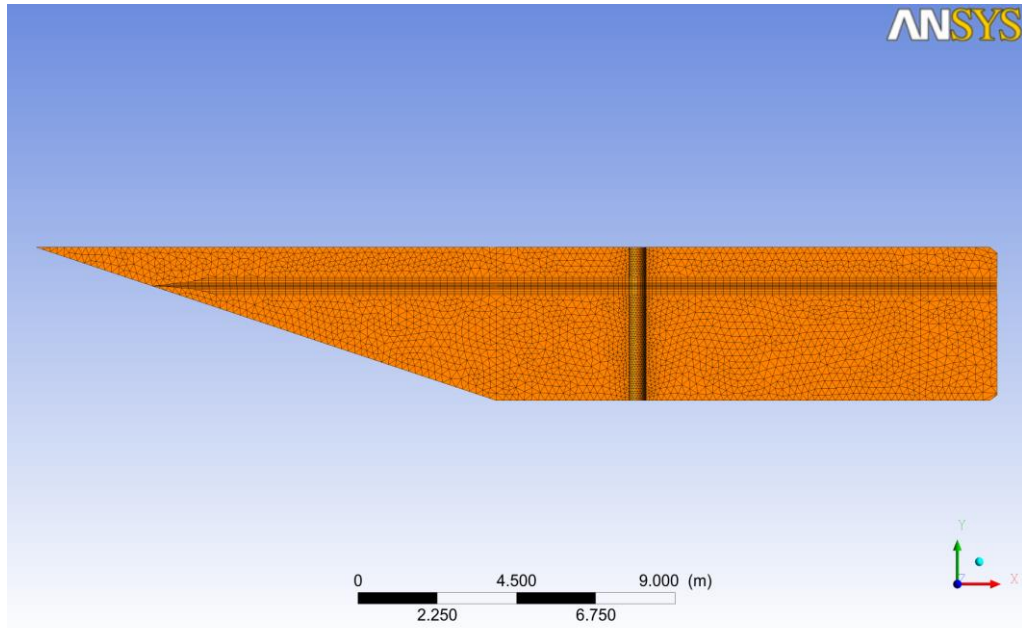


Figure 4.7 Mesh in case one

The bottom and the beach boundary was set to a no slip wall with $U_{wall} = 0$. The top boundary was set to an entrainment opening with zero static pressure in order to let the airflow in and out without any specific direction. The front was set to a slip wall, and the back boundary was set to symmetry plane. The piston or flap wavemaker was set to a no slip wall with prescribed motion from the wavemaker theory, see Figure 4.8.

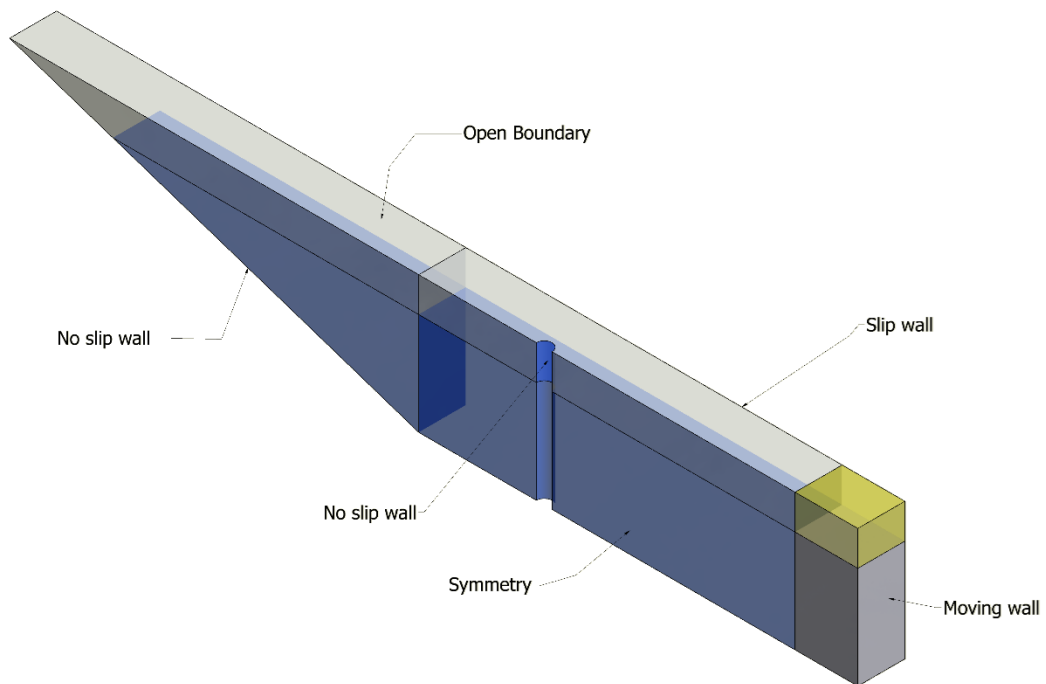


Figure 4.8 Model boundary conditions

4.2.5 CFX Expression Language

The formulas used to set up a simulation in CFX Pre can be expressed with the built in CFX Expression Language (*CEL*). In CFX there are many built in functions that can be used and combined to make own functions and expressions. *CEL* gives the user opportunities to, for example express new boundary conditions and fluid specifications, which is useful when modeling specific cases. In a numerical wave tank, the wave formulas can be expressed by *CEL* expressions. Refer to ANSYS CFX user manual ANSYS (2013) for more information regarding the *CEL* language and the built in functions available.

In order to capture the surface elevation at a given position as function of time, the *CEL* language was used. A cross sectional plane at the wanted position of the numerical wave gauge was made. From the definition of the volume fraction, which is defined 1 in the water phase, 0.5 at the free surface and 0 in the air phase, the vertical position of the free surface could be defined. The built in function *areaInt* was used to integrate the water volume fraction over the cross section. By dividing the area integral with the unit width of the tank and relocate the vertical position to the mean free surface position, the actual water height at the given time was found. In the solver, a defined *CEL* expression can be monitored. In that way, the surface elevation could be monitored during the analysis.

$$y(t) = \left(\frac{(\text{areaInt}(\text{water.VolumeFraction})@\text{section})}{b} \right) - h \quad (4.5)$$

In equation (4.5) the *areaInt* is a built in area integral function, *water.Volume Fraction* is the actual water volume fraction at a given *y* position, *section* is the studied cross sectional section and *h* is the water depth.

4.3 Validation Procedure (2D NWT without a monopile)

The ability of a numerical model in solving accurately a specific problem can be verified through validation process. The validation can be done through comparisons between numerical results against experimental or analytical ones. Unlike field tests, the tests laboratories have partial or entire control of the boundary conditions. However,

laboratory studies can become a difficult task, due to high cost, complexity of the physical phenomenon and difficulty, in boundary condition control observed in larger wave tanks. On the other hand, analytical models are attractive tools in numerical model validation to overcome the difficulty found in collecting experimental data. In spite of the analytical results are available for some problems, which have simpler domain and boundary conditions, they have been selected to numerical model validation for many investigators Agamloh, et al. (2008)[26], Finnegan and Goggins (2012) [1] and Lal and Elangovan (2008)[31]. Some analytical theories have been developed to represents the periodic water wave boundary value problem. The choice of the most suitable wave theory for a specific problem cannot be easily solved, since different theories could better reproduce distinct characteristics of the wave motion. Using the guidance of Finnegan and Goggins (2012) [1] linear wave theory (1st order theory) is valid for verification of the current work.

To simulate the generation and propagation waves in a numerical wave tank, a bi-dimensional computational domain section whose geometry is simpler than the real wave tank facility has been chosen. The domain is 35 meters long and 2.5 meters height with a water depth of 1.5 meters. Since CFX code does not have a two-dimensional solver, the domain was generated with one cell thick that is 0.10 meters wide see Figure 4.9. The validation case used for obtaining a NWT using CFX was based on the work of Silva, et al. (2010)[2].

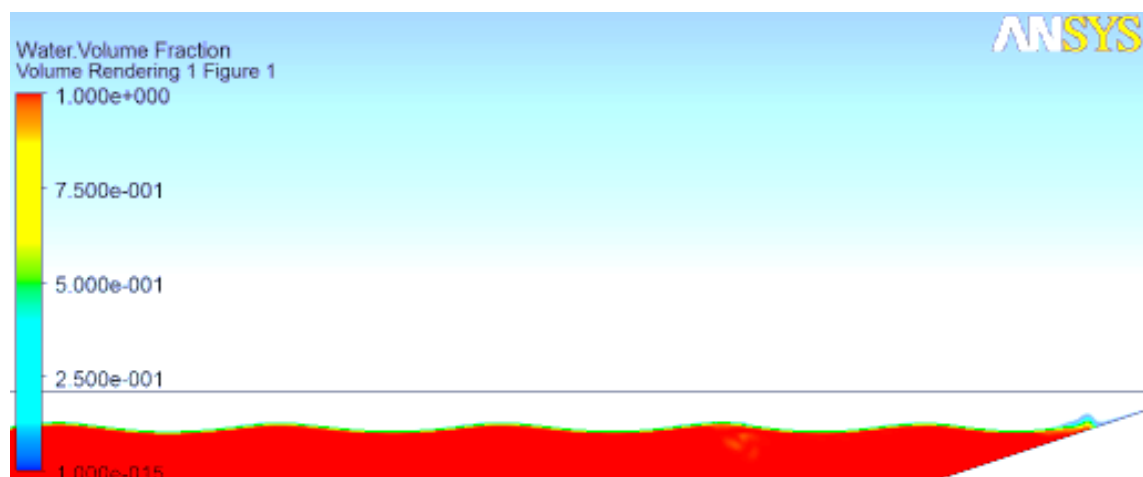


Figure 4.9 The NWT for the validation case

A NWT was constructed using CFX, the free surface elevation results were compared to Silva, et al. (2010) [2] results, see Figure 4.10. The results show a good agreement of the wave profile between CFX and analytical solution. This provides an evidence that CFX are capable of modeling wave using a wavemaker to produce waves. The next step is using the NWT to produce waves on structures, and study the effects of the interaction between the waves and the structures.

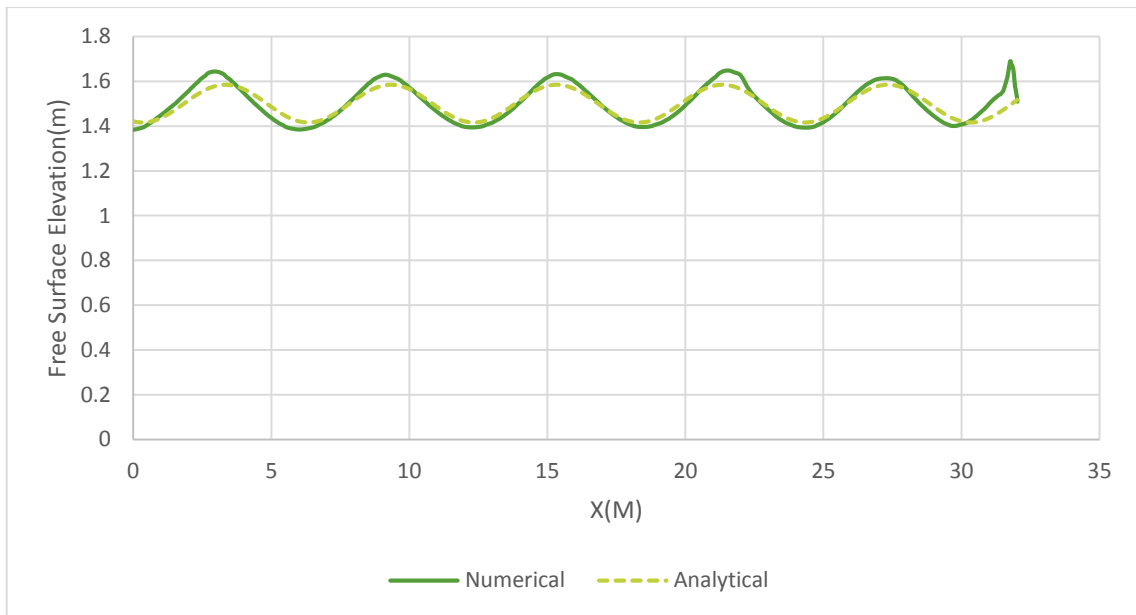


Figure 4.10 Silvia NWT Numerical vs. Analytical Wave Profile Solution $h=1.5\text{m}$, $L=6\text{m}$ at $t=60\text{ sec}$.

4.4 Identification of the Numerical Settings of the Proposed NWT

Four monopiles were used in this study, two monopiles' lengths of 4.35m and 3.25m were chosen to be investigated, the first is noted long and the second is noted short through this thesis. A periodic time of 1.96s was chosen for the wave and a wave length of 6m was chosen in order to have a wave steepness (H/L) of 0.095 which considered as a critical wave steepness, the wave produced is a critical wave lies between the deep and intermediate region.

An example of the four cases applied in this work is shown in the Figure 4.11. Similar to what in chapter 4, the domain length was $L_t = 27.05\text{m}$ which gave a free surface of 23.75m

with a beach slope of 1 : 3 at the domain end. The water depth was 3.25m and 1.1m air was modeled above. A 3D analysis was performed with an extruded length of 1.5m.

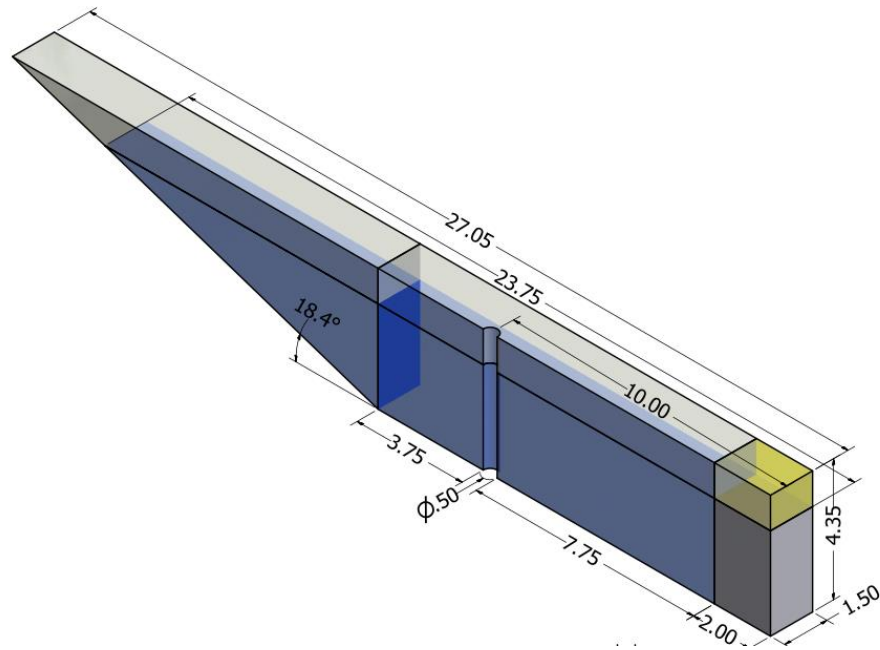


Figure 4.11 Domain of the first case. Similar domain was used for the other three cases.

Close to the free surface, a finer mesh was used in order to capture the free surface accurately and to try to achieve less variation in wave amplitude along the wave tank as commented earlier. Two meshing methods were used to achieve the required result. The first is the sizing method, where the minimum element size was introduced. The second is the inflation, which is applied on the surface between water and air, and used to link between the finer elements at the free surface and the rest of the elements away from the free surface.

The minimum element size was chosen according to equation (3.37); a minimum element size of 0.25m was used in the four cases.

Similar numerical parameters and boundary conditions used in chapter 4 that is; The domain was divided at $x = 2\text{m}$ in two sub domains. The bottom and the beach boundary was set to a no slip wall, $U_{\text{wall}} = 0$. The monopile was also set to a no slip wall. The top boundary was set to an entrainment opening with zero static pressure, the front was set to a slip wall, and the back boundary was set to symmetry plane. The piston wavemaker was

set as a moving no slip wall. The numerical parameters and settings are presented in Table 4.4.

Table 4.4 Numerical settings for the four cases

Parameter	Setting
Model	Transient
Turbulence	SST
Advection Discretization Scheme	Specified blend, blend factor =1
Time Discretization Scheme	Second order Backward Euler
Convergence criteria	RMS < 1E - 3
Convergence loops	2 - 6
Precision	Single
Mode	Serial
Total time	15s
Time step	$\Delta t = 0.02s$

At the monitor plane at $x=11m$ away from the wavemaker, water free surface elevation was logged. Both pressure forces and viscous forces was logged on the monopile. In addition also the torque around the y-axis was logged. The non-dimensional time step value was $T/\Delta t = 100$.

In Table 4.5, the related wave input parameters for the four performed cases are given.

Table 4.5 Wave input parameters

L(m)	h (m)	H(m)	k	ω	kh	H/L
6.000	3.250	0.45	1.047	3.202	3.403	0.095

Where L is the wave length, h is the water depth, H is the wave amplitude, k is the wave number = $\frac{2\pi}{L}$, and $\omega = \frac{2\pi}{T}$ is the frequency.

5 CHAPTER 5: COMPUTATIONS, RESULTS AND DISCUSSION

In this chapter, the numerical wave tank developed in chapter 4 has been used to perform a three dimensional analysis of wave forces on four monopiles. Similar wave amplitudes and wave periods used in the four runs to produce external wave forces on the monopiles. For the wave maker theory and linear wave theory, the same parameters were set to compare results against the numerical model.

5.1 Results and Discussion

All the four numerical simulations in this section was performed in serial on a local 64 – bit computer with an Intel® core™ i7 @2.20GHz processor and 8GB installed memory. Two main results were obtained from the four runs; the wave free surface elevation and the force-moment results.

5.1.1 Wave free surface elevation

Wave Elevation, of the four cases, was measured at a plane lies at $x=11$ m away from the wavemaker as shown in Figure 5.1.

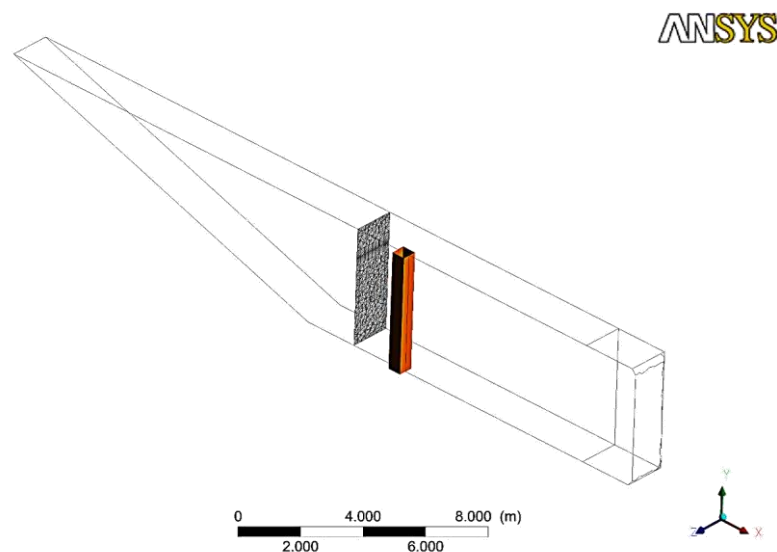


Figure 5.1 Model with the plane used to monitor wave elevation at $x=11$ m away from the wavemaker is shown

The CFD results obtained at the investigation plane lies at $x=11$ m away from the wavemaker, and lies after the position of the monopile, this was to avoid any turbulences caused by it.

The applied size of the mesh used was based on the optimum size noted by [1], a maximum edge length of 0.25m per element was chosen, and a tetrahedron element was used for this case. The mesh was condensed around the monopile to gain a better result, and to account for the curvature of the surface of the monopile. The mesh was condensed around the free surface in order to have a better wave profile as shown in Figure 5.3. The total number of mesh elements in case one is 173,77 elements.

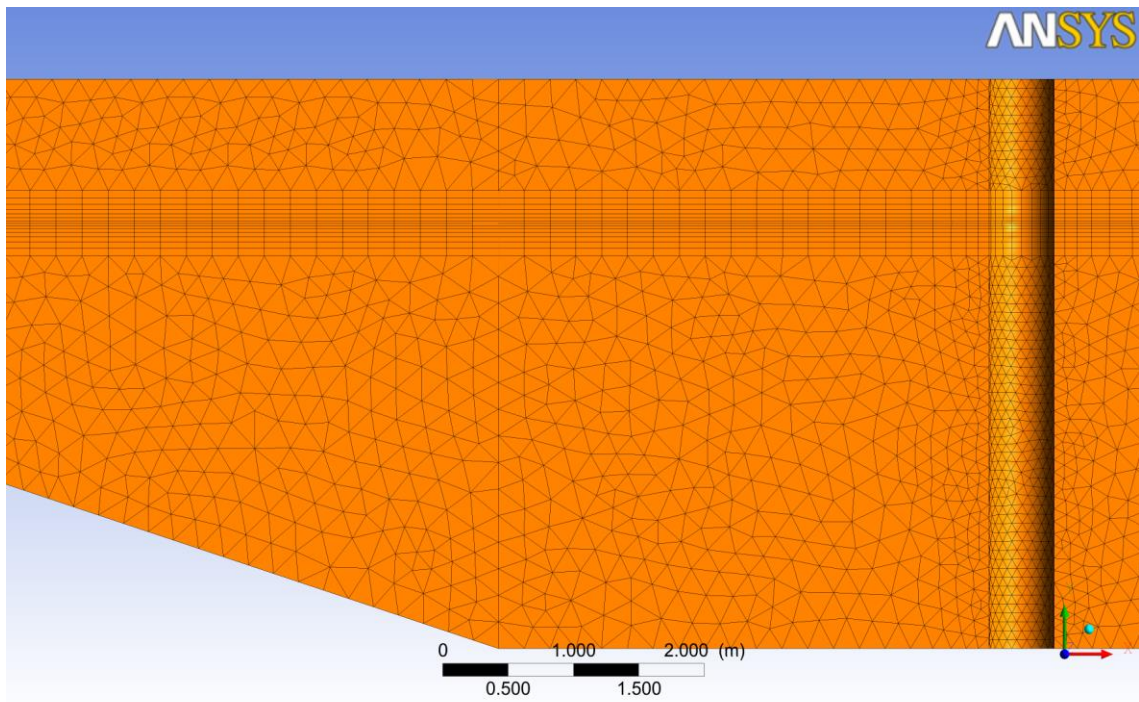


Figure 5.3 Mesh in case one

The boundary conditions for case one is the same as stated in the previous chapter. Open boundary was used for the top. No-slip walls used for the monopile, the side wall and the beach. Symmetry was used for the other side of the NWT.

5.1.3.1 Wave elevation measurement

The elevation of the wave surface was measured at the investigation plane $x=11\text{m}$. As shown in Figure 5.4. The characteristics of the generated wave using CFX agrees with the analytical wave. The values of CFX wave at the early time (approximately less than 6 seconds) seems to be very small, this is because the wave is still generating, and a full developed wave did not reach the investigation plane. The values of the amplitude of the

CFX wave is less than the values of the analytical wave with an average difference of 0.6%¹.

Another characteristic is the frequency of the wave, which shows a very strong agreement between the CFX and the linear results. The CFX and linear wave gives approximately the same frequency.

A good agreement is also obtained indicating that the assumptions of using linear wave theory was reasonable. Note that by using linear wave theory, a small deviation is found around the crest and trough of the wave. The chosen wave amplitude in the theoretical wave elevation is taken from the actual measured wave amplitude from the CFD analysis at $x=11m$. Only a change in the kx value in the theoretical surface elevation expression was done.

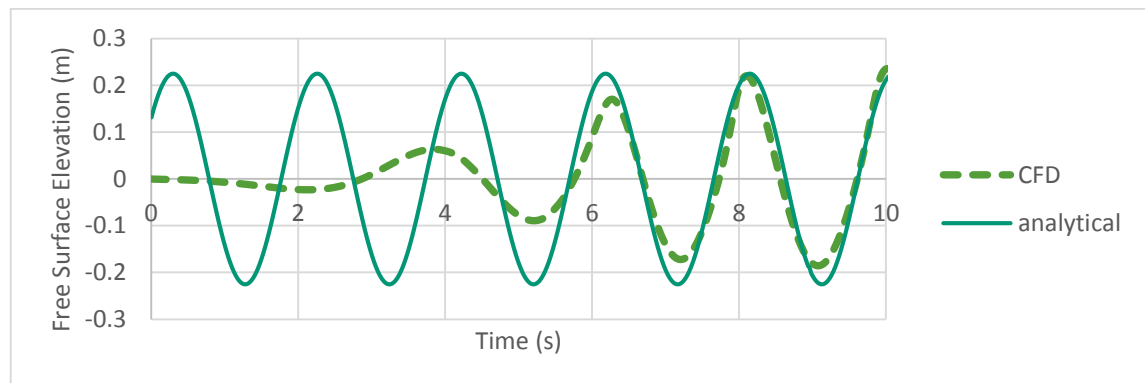


Figure 5.4 Free surface elevation for Case 1 compared with Linear wave theory, measured at $x=11$ m from the wavemaker

5.1.3.2 Force and moment measurement

The reason of this study is to investigate the waves loading on monopiles. As shown in Figure 5.5, results of total forces on case one monopile are compared with Morison's equation results.

¹ The values with time less than 6 seconds were excluded from the comparison because it is not representative.

CFX forces at early time (i.e. less than 5 seconds) seems not to agree with Morison's equation due to the lack of wave development at that stage.

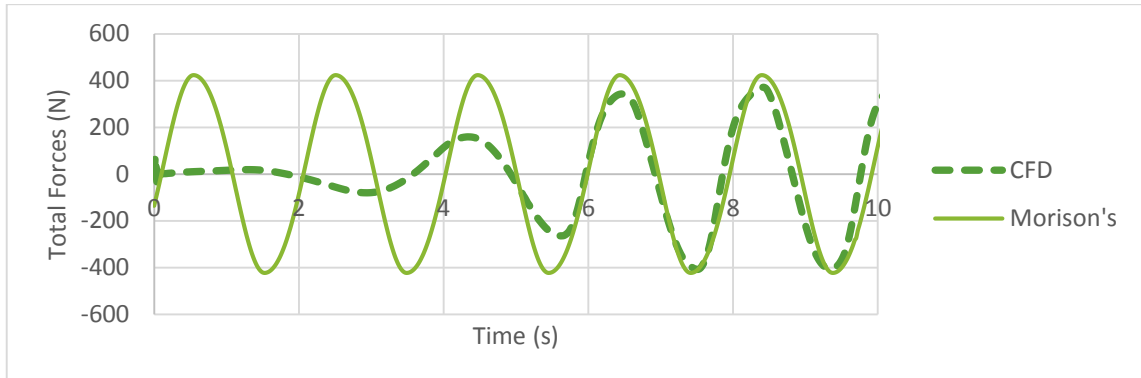


Figure 5.5 Comparison of total force acting on monopile for Case1 between CFD and Morison's equation

CFX results after $t=5$ seconds agrees with Morison's equation in frequency, but the values of the total forces of CFX are less than Morison's. The reason behind this difference is the different mathematical models of CFX and Morison's. Morison's equation depends on the coefficients of drag and inertia which is chosen as $C_d=1$ and $C_m=0.95$, respectively according to Techet (2004) [52] for the purpose of gaining a rough estimate of the total force on the monopile. In contrast, CFX depends on solving Navier Stokes equations, which considered as the general governing equation for the fluid behavior Pengzhi (2008)[3]. Hence, NSE seem to give more realistic results than Morison's does. Using NSE for the purpose of obtaining total forces is more economical than Morison's equation, since it give less total force values and yet more realistic.

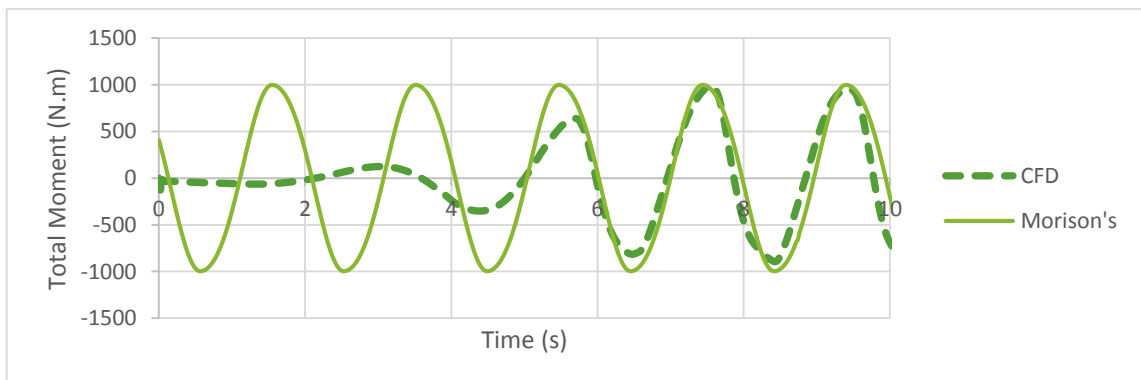


Figure 5.6 Comparison of total moment around seabed acting on monopile for Case 1 between CFD and Morison's equation

The total moment on case one monopile is calculated around the seabed. Moments in whether the CFX or Morison's case are resulted from the product of the resultant force acting on the monopile times the distance from the seabed to the position of the resultant. As it is shown in Figure 5.6, the CFX and Morison's results fluctuated with the same frequency, however, the values of the moments of CFX seem to be less than Morison's. Because moments reflect the total force results, since they are produced from the total force multiplication with its lever arm. Moreover, the total forces results showed that CFX values are less than Morison's and hence the moment's values of CFX are less than Morison's values.

5.1.4 Results of case two: short circular-cross section monopile

The second case studies the effect of a regular water wave on a monopile of a length of 3.25m which is shorter than the length of monopile in case one, with a cross section of a circle with a diameter of 0.5m as shown in Figure 5.7.

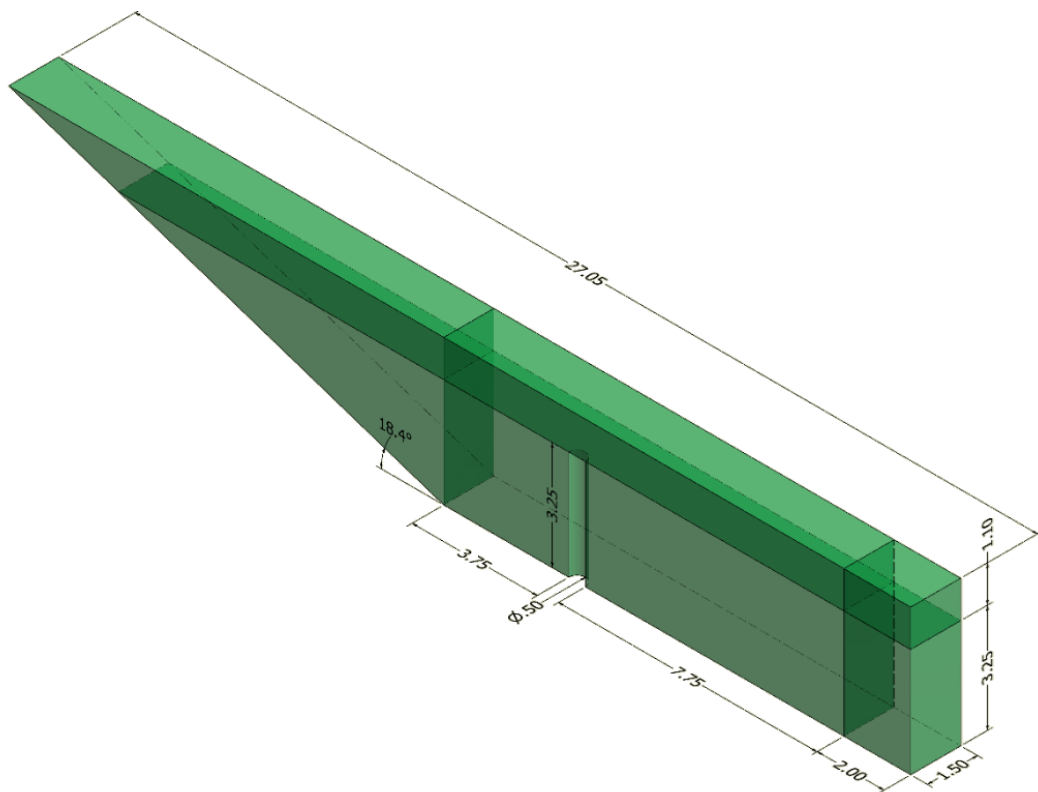


Figure 5.7 Geometry of the second case

The size of the mesh used was based on the optimum size noted by Finnegan and Goggins (2012)[1], a maximum edge length of 0.25m per element was adopted, and a tetrahedron

element was used for this case. The mesh was condensed around the monopile to gain a better result, and to account for the curvature of the surface of the monopile. The mesh was condensed around the free surface in order to have a better wave profile, see Figure 5.8. The total number of mesh elements in this case is 171,344 elements.

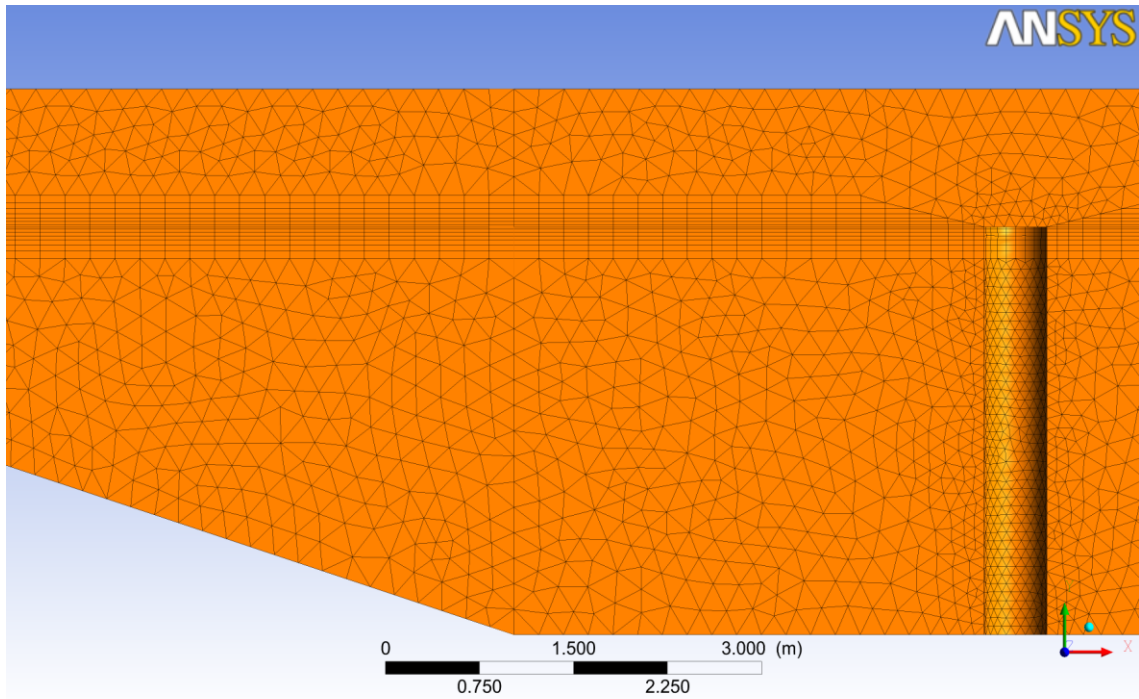


Figure 5.8 Mesh in case two

The boundary conditions for case two is the same as stated in the previous chapter. Open boundary was used for the top. No-slip walls used for the monopile, the sidewall and the beach. Symmetry was used for the other side of the NWT.

5.1.4.1 Wave elevation measurement

The elevation of the wave surface was measured at the investigation plane $x=11\text{m}$, as shown in Figure 5.9. The characteristics of the generated wave using CFX agrees with the analytical wave. The values of CFX wave at the early time (approximately less than 6 seconds) seems to be very small, this is because the wave is still generating, and a full developed wave did not reach the investigation plane.

Another characteristic is the frequency of the wave, which shows a very strong agreement between the CFX and the linear results. The CFX and linear wave gives approximately the same frequency.

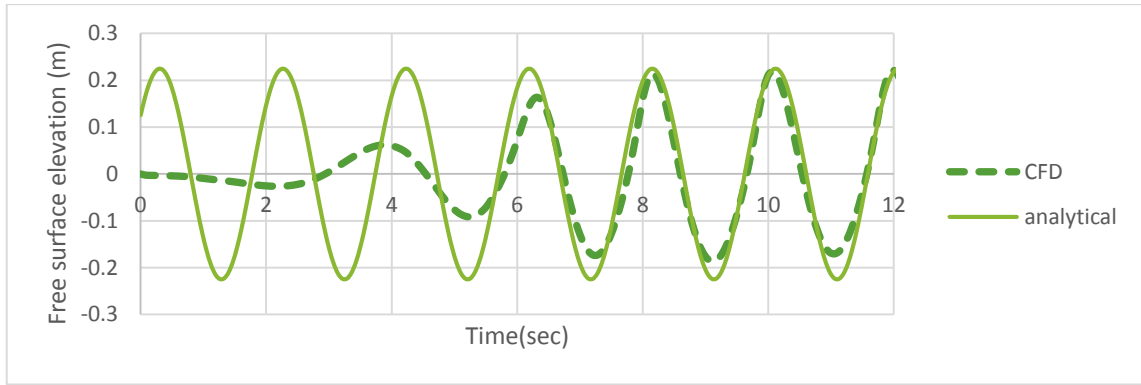


Figure 5.9 Free surface elevation for Case 2 compared with Linear wave theory, measured at $x=11$ m from the wavemaker

5.1.4.2 Force and moment measurement

As shown in Figure 5.10, results of total forces on case one monopile are compared with Morison's equation results.

CFX forces at early time (i.e. less than 5 seconds) seems not to agree with Morison's equation due to the lack of wave development at that stage.

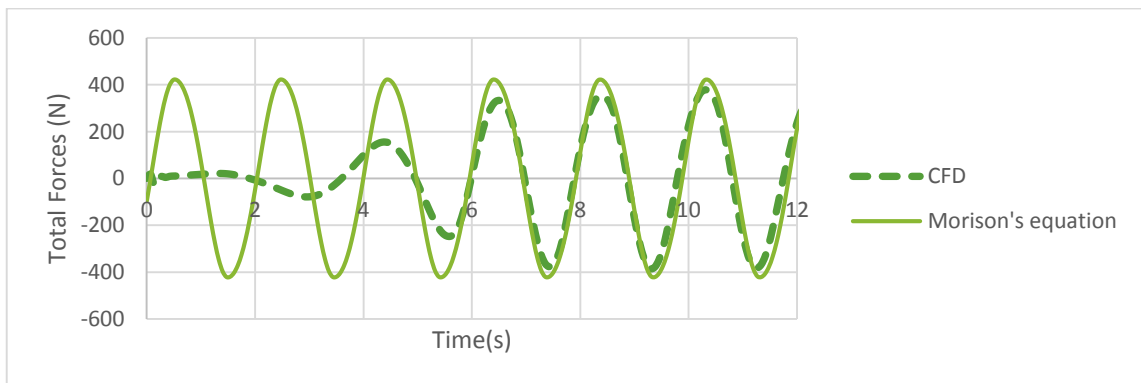


Figure 5.10 Comparison of total force acting on monopile for Case 2 between CFD and Morison's equation

The behavior of case two monopile does not differ much than that of case one. The reason is the total forces of the two cases are approximately identical, in case one a 3.25m of its length is exerted to water and the rest 1.1m is exerted to air and in case two the whole length of 3.25m is exerted only to water. Since the air forces are insignificant compared to water, both cases gave almost the same results.

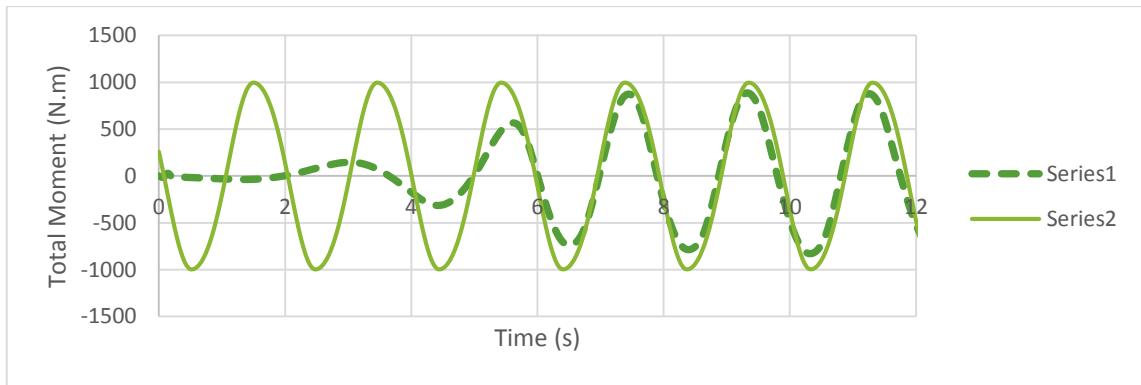


Figure 5.11 Comparison of total moment about seabed acting on monopile for Case 2 between CFD and Morison's equation

As it is shown in Figure 5.11, the CFX and Morison's results fluctuated with the same frequency, however, the values of the moments of CFX seem to be deviated from the mean value.

5.1.5 Results of case three: long square-cross section monopile

The third case studies the effect of a regular water wave on a monopile of a length of 4.35m with a cross section of a square with a side edge length of 0.5m as shown in Figure 5.12.

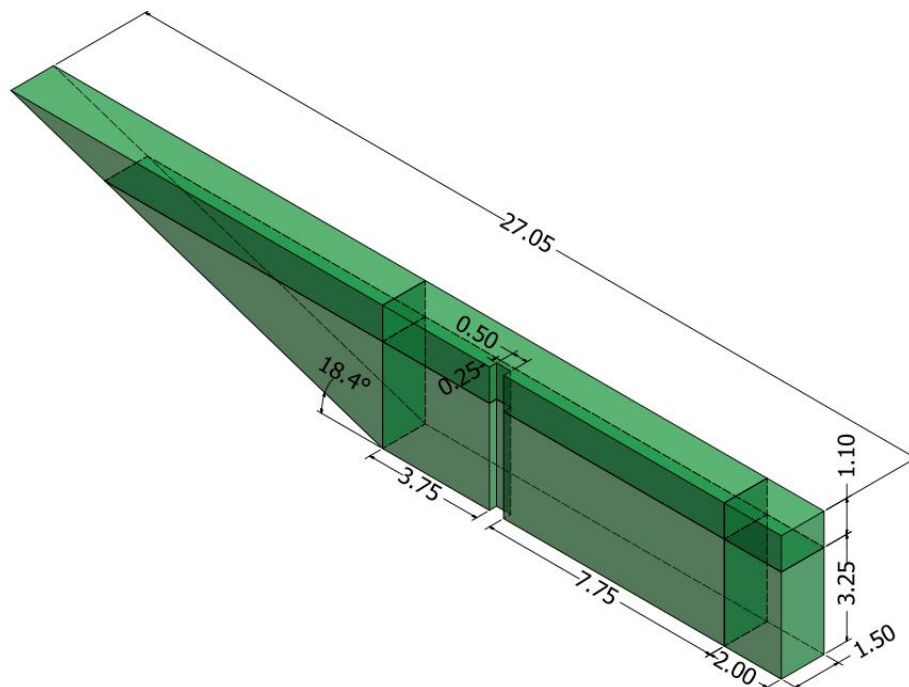


Figure 5.12 Geometry of the third case

The geometry was modeled using ANSYS DesignModeler, as stated above, a beach slope of 1:3 is needed for damping the wave and not to let it reflect and affect the results, this is obvious in the above figure.

As in the previous cases the size of the mesh used was based on the optimum size suggested by Finnegan and Goggins (2012)[1], a maximum edge length of 0.25m per element was used, and a tetrahedron element was used for this case. A total number of mesh elements used is 158,733. The mesh was condensed around the monopile to account for the sharp angles of the monopile shape. The mesh was condensed around the free surface in order to have a better wave profile see Figure 5.13.

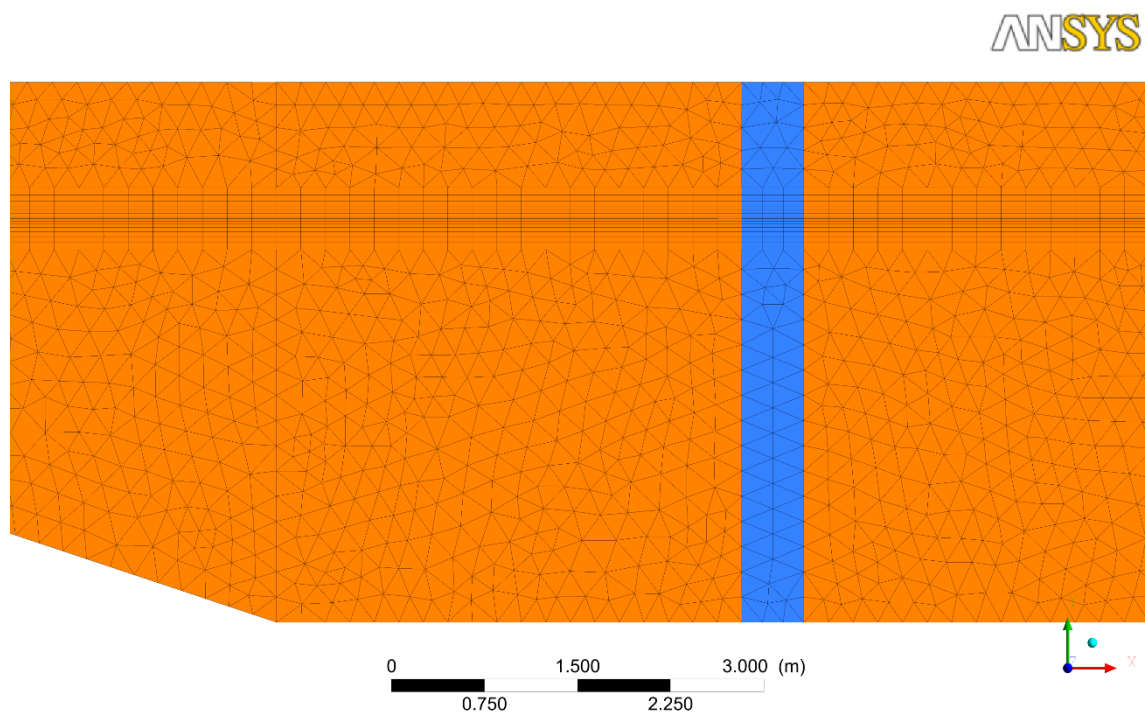


Figure 5.13 Mesh in case three

The boundary conditions for case three is the same as stated in the previous chapter. Open boundary condition was used for the top. No-slip walls used for the monopile, the sidewall and the beach. Symmetry was used for the other side of the NWT.

5.1.5.1 Wave elevation measurement

Figure 5.14 presents the comparison between CFX and analytical results, as indicated in the previous cases, a very good agreement between the two solutions is gained.

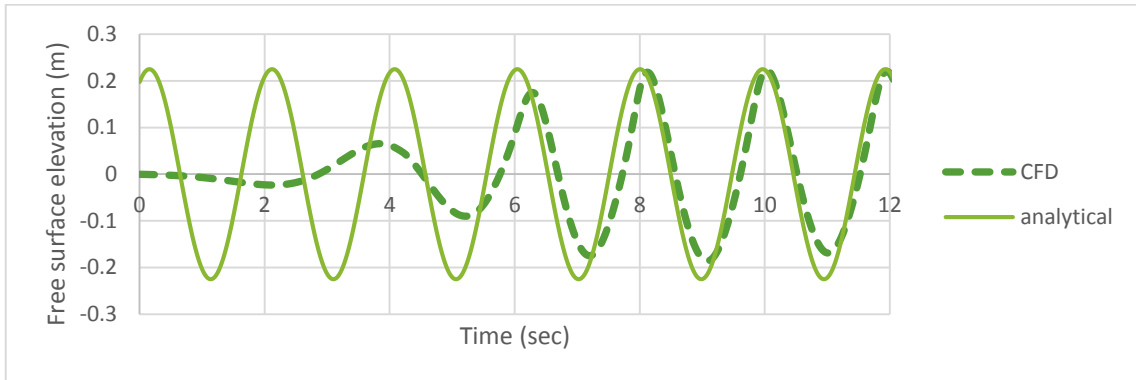


Figure 5.14 Free surface elevation for Case 3 compared with Linear wave theory, measured at $x=11$ m from the wavemaker

5.1.5.2 Force and Moment Measurement

The behavior of the square cross section monopile when it is exerted to fluid differs from the circular cross section due to the difference in the drag coefficient, the drag coefficient of the square cross section is greater than the circular, and hence the total forces acting on the square cross section monopile is greater as shown in Figure 5.15. Later in this chapter, a detailed investigation of the effect of cross section on the total forces will be discussed.

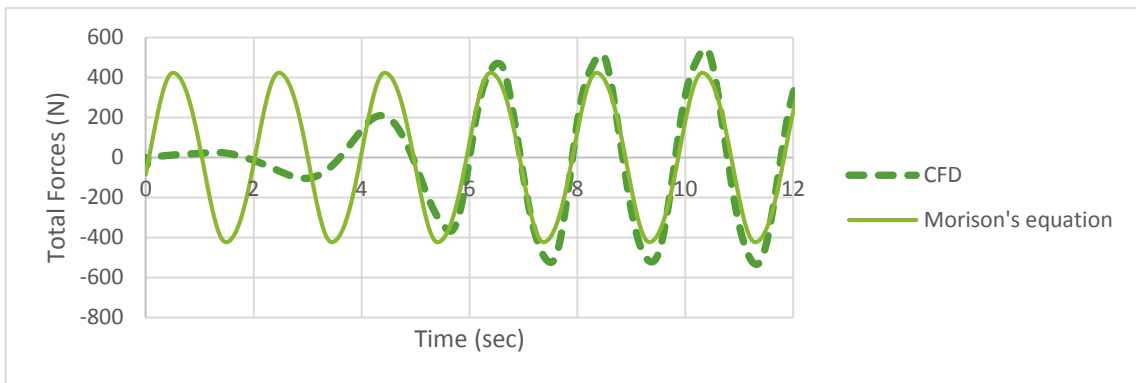


Figure 5.15 Comparison of total force acting on monopile for Case 3 between CFD and Morison's equation

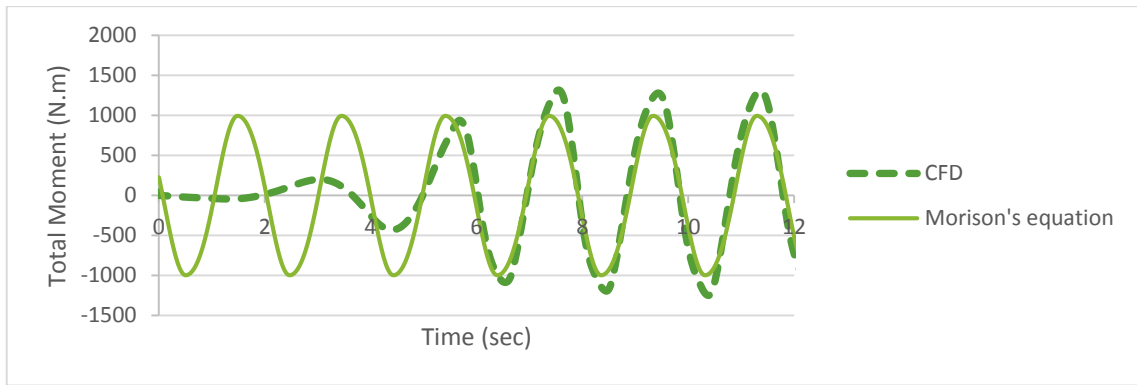


Figure 5.16 Comparison of total moment about seabed acting on monopile for Case 3 between CFD and Morison's equation

The moment graphs show a reflection of the total forces on the monopile. A good agreement between CFX and Morison's equation is obtained as seen in Figure 5.16.

5.1.6 Results of case four: short square-cross section monopile

The fourth case studies the effect of a regular water wave on a monopile of a length of 3.25m with a cross section of a square with a side edge length of 0.5m as shown in Figure 5.17.

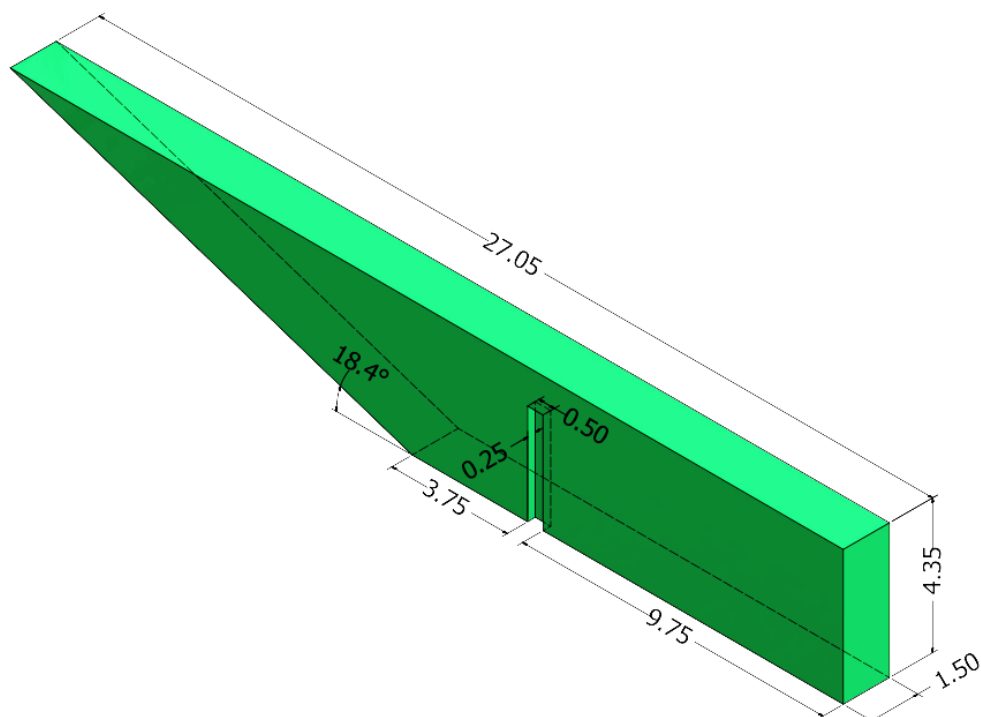


Figure 5.17 Geometry of the fourth case

The geometry was modeled using ANSYS DesignModeler, as stated above a beach of slope 1:3 is needed for damping the wave and not to let it reflect and affect the results.

The size of the mesh used was based on the optimum size noted by Finnegan and Goggins (2012)[1], a maximum edge length of 0.25 per element was used, and a tetrahedron element was used for this case. The mesh was condensed around the monopile to gain a better result, and to account for the curvature of the surface of the monopile. The mesh was condensed around the free surface in order to have a better wave profile, see Figure 5.18. The total number of mesh elements in this case is 269,975 elements.

ANSYS

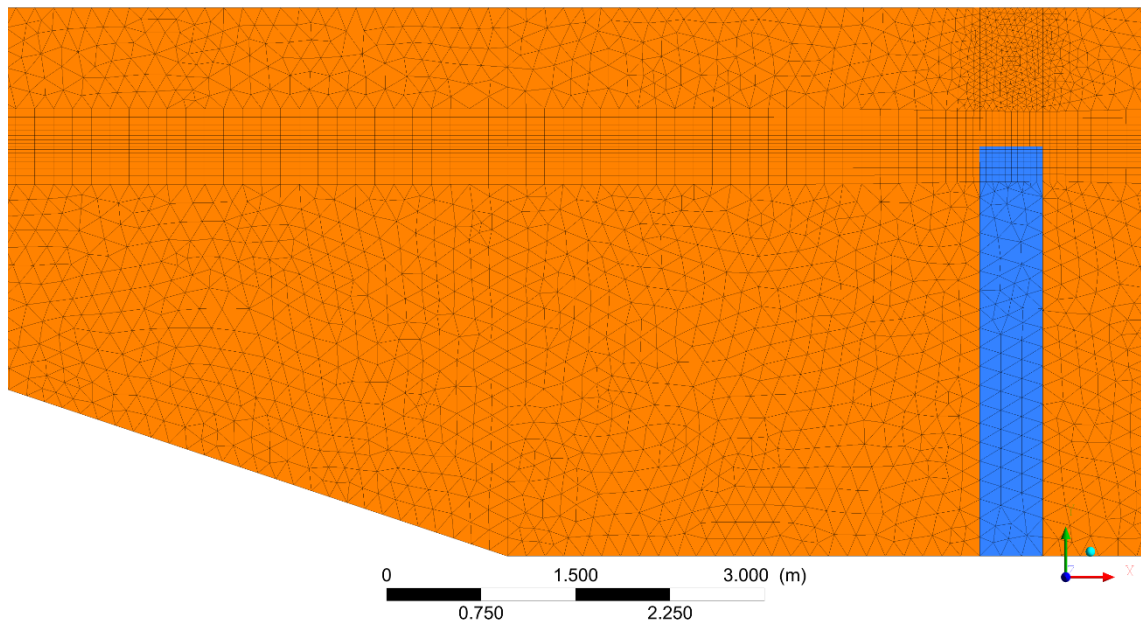


Figure 5.18 Mesh in case four

The boundary conditions for case four is the same as stated in the previous chapter. Open boundary was used for the top. No-slip walls used for the monopile, the sidewall and the beach. Symmetry was used for the other side of the NWT.

5.1.6.1 Wave elevation measurement

The elevation of the wave surface was measured at the investigation plane $x=11\text{m}$. As shown in Figure 5.19. The characteristics of the generated wave using CFX agrees with the analytical wave. The values of CFX wave at the early time (approximately less than

6 seconds) seems to be very small, this is because the wave is still generating, and a full developed wave did not reach the investigation plane.

Another characteristic is the frequency of the wave, which shows a very strong agreement between the CFX and the linear results. The CFX and linear wave gives approximately the same frequency.

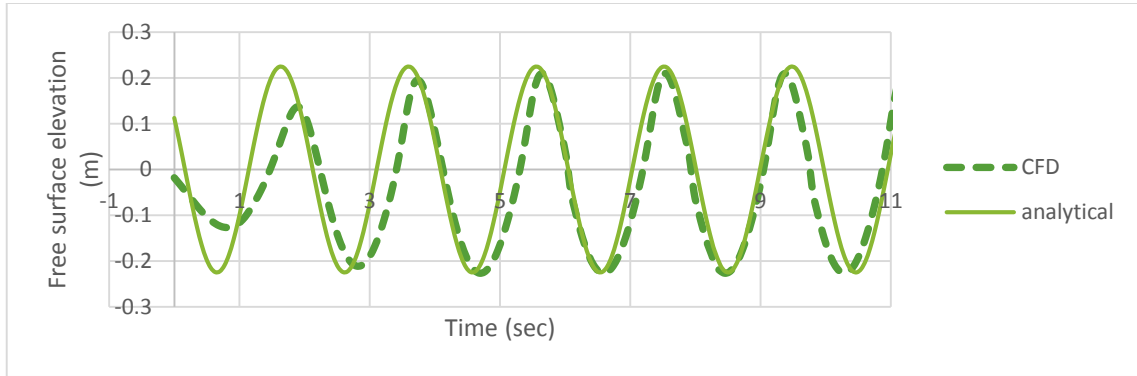


Figure 5.19 Free surface elevation for Case 4 compared with Linear wave theory, measured at $x=11$ m from the wavemaker

5.1.6.2 Force and moment measurement

Figure 5.20 **Error! Reference source not found.** presents a comparison between CFX and Morison's results; an excellent agreement between both CFX and analytical solutions in terms of the values and frequency is obvious. Although in case four the monopile was fully submerged in the fluid it gave a similar results with its former case three. Whether in case 3 or in case 4 the submerged length of the monopile is identical, and since there is no significant effect of air forces on monopile, the results of total forces on the monopiles of case 3 and case four are the same.

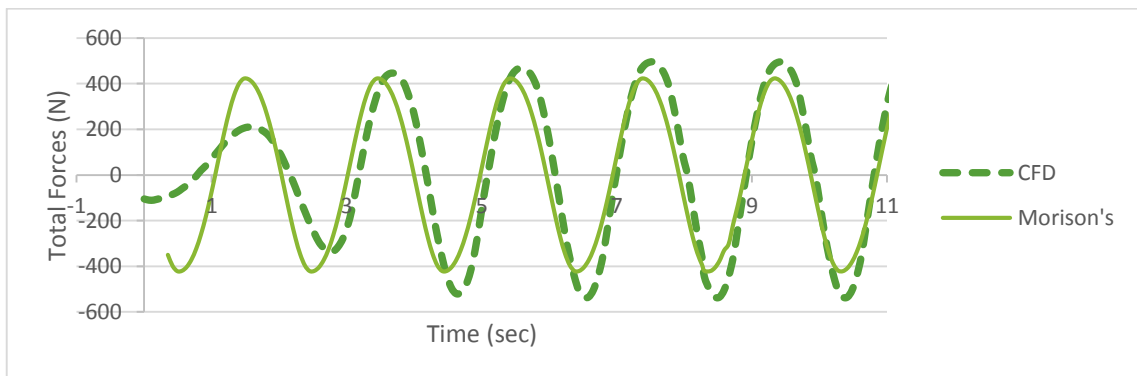


Figure 5.20 Comparison of total force acting on monopile for Case 4 between CFD and Morison's equation

The moment graphs show a reflection of the total forces on the monopile. A good agreement between CFX and Morison's equation is obtained as seen Figure 5.21, the reason of the deviation of the numerical results may be the coarseness of the mesh, and the effect of the interaction between the top of the monopile and the free surface of the wave.

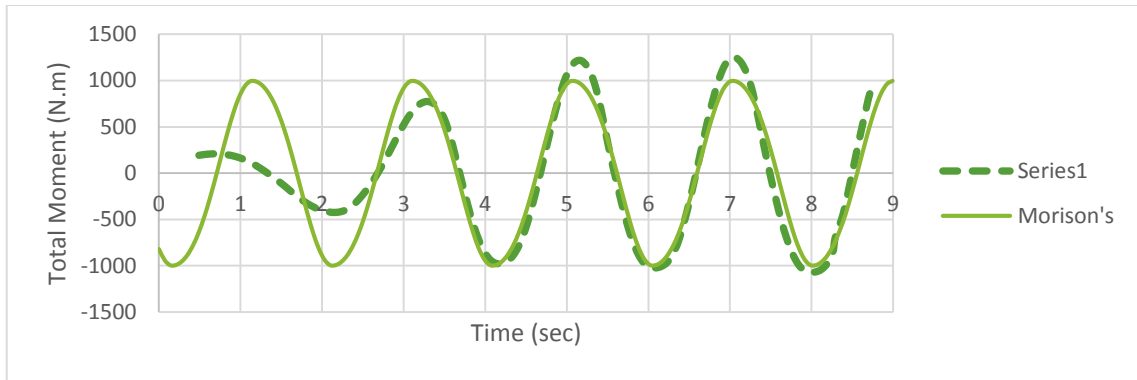


Figure 5.21 Comparison of total moment about seabed acting on monopile for Case 4 between CFD and Morison's equation

5.2 Effect of monopile length on total hydrodynamic forces

The effect of several monopile lengths on the impact on the total forces on them is investigated. A comparison between the total subjected forces at the short and long circular monopiles is presented in Figure 5.22, and for the long and short square is seen in Figure 5.23.

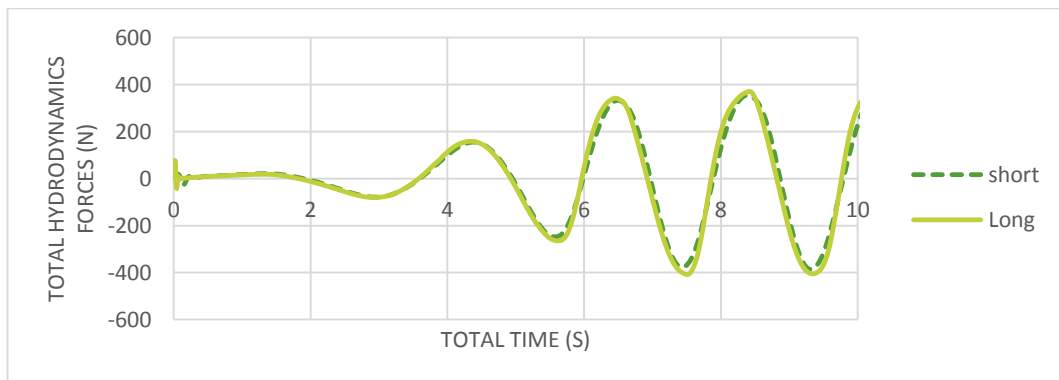


Figure 5.22 Forces on long and short Circular Monopiles

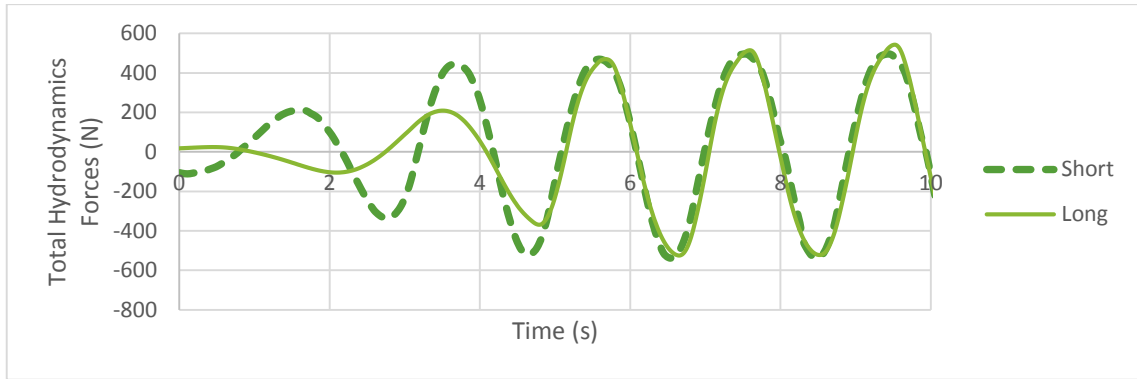


Figure 5.23 Forces on long and short Square Monopiles

The above figures indicates a significant agreement of the results whether the length of the monopile was 4.35m or 3.25m. This was due to the fact that the upper part of the longer monopiles lies in air, which, in fact, has no significance forces acting on the monopiles. Figure 5.24 and Figure 5.25 show the force distribution on a long and short monopiles respectively, it is obvious from the results that the total forces acting on the upper part of the longer monopiles are close to zero, while the short monopile lies directly beneath the free surface, giving identical total forces for the two cases.

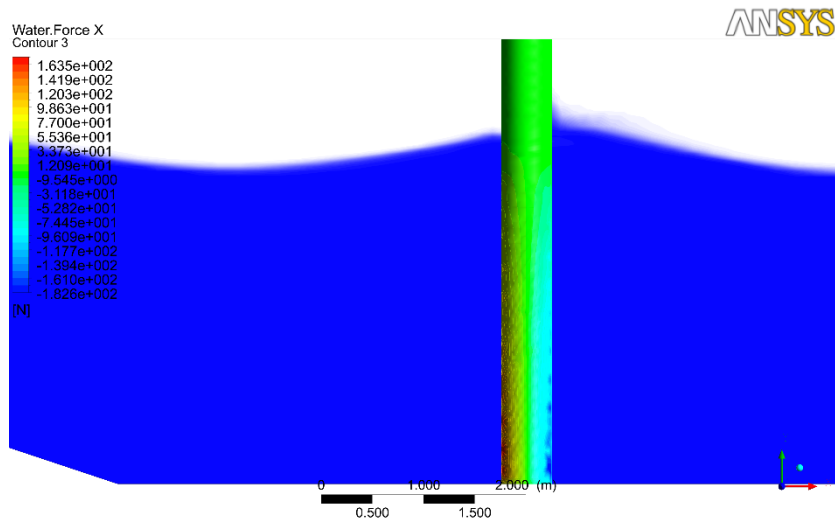


Figure 5.24 Forces distribution on case I monopile

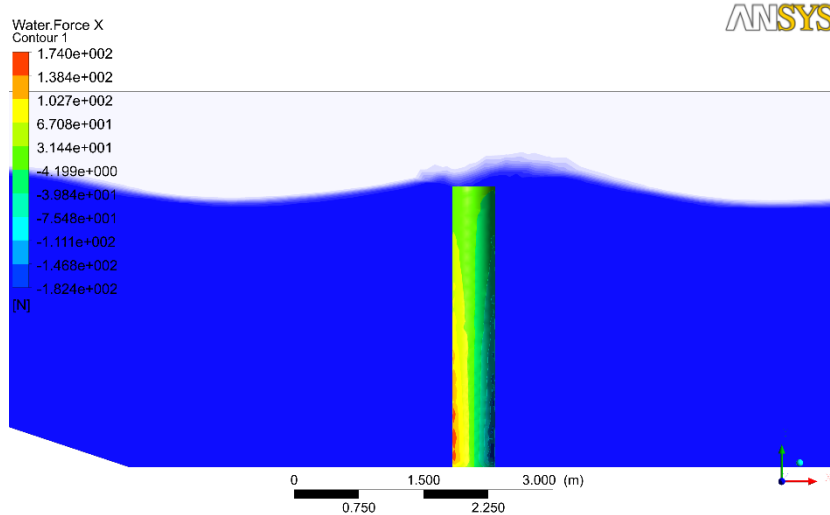


Figure 5.25 Forces distribution on case II monopile

5.3 Effect of monopile cross section on total hydrodynamic forces

The effect of several monopile cross section shapes on the impact on the total forces on them is investigated. A comparison between the total subjected forces at the square and circular monopiles is presented. As seen in Figure 5.26, the velocity streamlines and vectors around circular cross section shape are connected, and smooth, which means it has a low drag coefficient. This leads to lower total forces acting on the circular cross section monopiles.

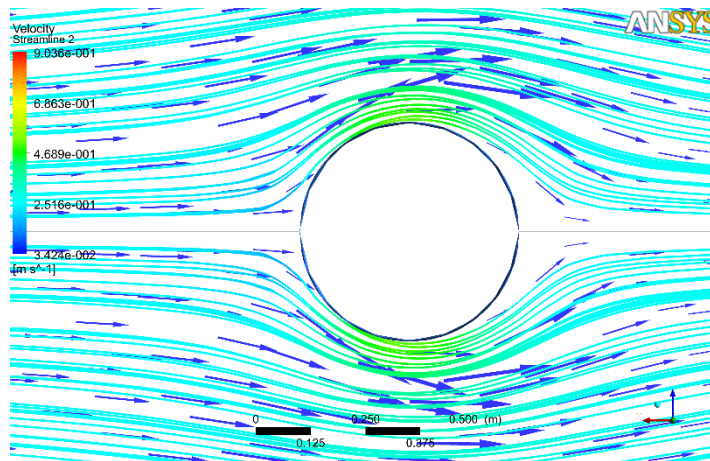


Figure 5.26 Velocity streamlines and vectors around circular monopile at elevation=2.5m, time= 9.6 s

Figure 5.27 shows a separation of the streamlines on the edges of the square cross section. The existence of sharp angles in the square section causes an increase in the coefficient

of drag, which will reflect on the total forces on the square section monopile. Hence, for the same amount of material the circular cross section monopile will resist higher forces values than square cross section monopile.

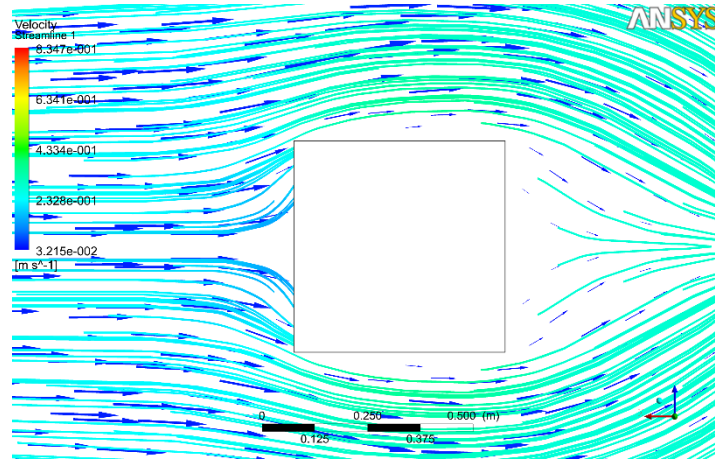


Figure 5.27 Velocity streamlines and vectors around square monopile at elevation=2.5m, time= 9.6 s

5.4 Comparison of the free surface elevation of the four cases

At the studied plane at $x=11\text{m}$, the water was assumed unaffected by the monopiles. The CFD results of the free surface elevation shown in Figure 5.28 gave approximately the same values. This indicates that the four runs were very close; the investigation plane took place a distance beyond the position of the monopile, the reason for this is to let the wave recover from any disturbances caused by the occurrence of the monopile.

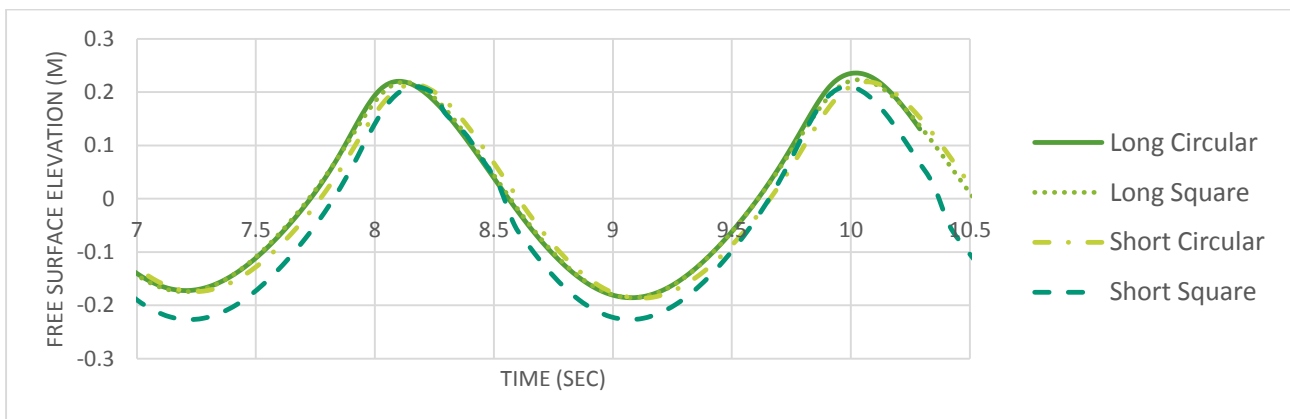


Figure 5.28 Comparison of the free surface elevation in the four cases at $x=11\text{m}$

6 CHAPTER 6: CONCLUSION AND RECOMMENDATIONS

6.1 Modeling of the NWT

Navier Stokes equations (NSE) are solved numerically using ANSYS CFX, which uses the Volume of Fluid method (VOF). The VOF method is the widest used method in CFD software since it is stable and cut for modeling fluids because it deals easily with volumes, it is better than other numerical methods such as Finite Difference Method or Finite Element Method[32].

The CFX software was used to produce a NWT to be validated with the previous work of[2]. After validating the ability of CFX to produce NWT, it was used for modeling the current problem.

The free surface elevation results of the models obtained from CFX were compared to the analytical linear wave theory, the forces results of CFX were compared to the semi-empirical Morison's equation. Morison's equation [44] was adopted by many offshore structures design guidelines [4] to obtain the forces of waves on fixed vertical cylinders, but it is unfortunately limited to cylinders with circular cross sections, and only with slender cylinders. Another limitation of Morison's is the need to obtain the coefficient of drag and the coefficient of inertia, which is related to Reynolds number, this will need a full size experiment of the pile, hence the use of Morison's gives a rough estimate of the wave forces.

The use of CFX, in contrast with using analytical or semi-empirical models, is unlimited. Whichever the size or shape of the structure can be modeled with CFX easily, no coefficients or any other special settings is needed, but the problem with the numerical modeling is the huge computational effort needed to get the results, and the lack of experimental results needed to validate the work.

6.2 Conclusion

The modeled numerical wave tank from chapter 4 has been used to study wave forces on the four cases. Constant wave period 1.96s for the four cases was used. The wave elevation at $x = 11\text{m}$ gave good results compared with 1st order wave theory. The number of mesh elements was optimized by the suggestion of Finnegan and Goggins (2012) [1]to

give the most accurate results with least time of solution; this could be one reason for the obtained small variation in the wave elevation along the tank. The studied wave amplitude of $H=0.45\text{m}$ gave a linear wave profile. At the investigation plane $x=1\text{m}$, free surface elevation was monitored and logged. The time series of the free surface elevation gave good results compared with 1st order theory. Forces was calculated on the studied monopiles. Both the total force, pressure force and viscous force were determined. The viscous forces was obtained to be very small and can be neglected. The total force gave good results compared with the calculated theoretical force based on Morison's equation. In the theoretical approach, a drag coefficient of $C_d=1$ and a coefficient of inertia $C_m=0.95$ were used for the four cases. The CFD and theoretical results showed good agreement, Moments of the four cases showed a good agreement between CFD and theoretical results. The CFD results showed irregularity for the short monopiles due to the disturbance occurred between the free surface and the monopiles.

The use of CFX in modeling wave-structure interaction problem has been achieved. The conclusions can be summarized as follows:

- ❖ General conclusions about using ANSYS CFX for modeling wave-structure interaction
 1. The ANSYS CFX is a general-purpose fluid solver, that can be efficiently used to solve any problem contains fluid with the appropriate settings.
 2. ANSYS CFX can be a valuable tool for the ocean engineering and wave energy industries. It has been shown that ANSYS CFX can be used to successfully model a numerical wave tank if conditions and parameters of ANSYS CFX are appropriately set.
- ❖ Conclusions drawn from modeling wave-structure interaction in the four cases
 1. The monopiles were successfully modeled and reliable results with minimum deviation were obtained.
 2. The square cross section monopiles were modeled and gave rational results, since the square shape have greater drag coefficient than circular.

6.3 Recommendations

Based on the achievements and work of current research, the author recommends studying several areas of improvement that may be targeted for future work.

1. The numerical wave tank could be improved by developing a time independent method of preventing reflection, allowing longer simulation times.
2. Further experimental validation of the behavior of the numerical wave tank may be possible if waves are simulated and compared to experimental data sets.
3. Other modeling approaches could be used to simulate the NWT, and for example, meshless method such as Smoothed Particle Hydrodynamics (SPH) could be used to investigate FSI problems.
4. A more realistic representation of the waves could be used instead of the simple linear theory, for example, non-linear wave models are opt for modeling purposes due to its similarity with the conditions of real sea waves.
5. An independent study of the effect of the NWT width on the hydrodynamics forces acting on the monopile must be conducted, to know the optimum width of the NWT while keeping the computational effort to the minimum.
6. A study of the representation of the monopiles as a group is recommended to deduct the effects of different group formations and spacing between monopiles on the loads acting on them.

With further development of this work, it is believed that the potential is huge to model a floating wave energy device or floating coastal structure.

REFERENCES

1. Finnegan, W. and J. Goggins, *Numerical simulation of linear water waves and wave–structure interaction*. Ocean Engineering, 2012. **43**(1): p. 23-31.
2. Silva, M.C., et al. *Numerical Simulation of monochromatic wave generated in laboratory: Validation of a CFD code*. 2010. Rio de Janeiro: 23 Congresso Nacional de Transporte Aquaviário, Construção Naval e Offshore.
3. Pengzhi, L., *Numerical Modeling of Water Waves*. 2008, New York: aylor & Francis Routledge.
4. Chakrabarti, S.K., *Handbook of Offshore Engineering*. 2005, Plainfield, Illinois, USA: Elsevier.
5. Mo, W., et al., *A 3D Numerical Model for Computing Non-breaking Wave Forces on Slender Piles*. Journal of Engineering Mathematics 2005: p. 1-14.
6. Hughes, S.A., *Physical Models and Laboratory Techniques in Coastal Engineering*. World Scientific, 1993. **7**(1): p. 1-17.
7. Chakrabarti, S., *Offshore Structures Modeling*. World Scientific, 1994. **1**(1): p. 50-62.
8. *Coastal Landscapes: Forms and Processes*. 2014 [cited 2014; Available from: <http://clasfaculty.ucdenver.edu/callen/1202/Landscapes/KarCoast/Coastal/CoastalLandscapes.htm>].
9. Hasselmann, S., et al., *The WAM model—a third generation ocean wave prediction model*. J. Phys. Oceanogr, 1988. **1**(18): p. 1775–1810.
10. Tolman, H.L., *User manual and system documentation of WAVEWATCH-III version 1.18*. 1999, Environmental Modeling Center: Washington D C. p. 1-22.
11. Ris, R.C., N. Booij, and L.H. Holthuijsen, *A third-generation wave model for coastal regions, Part II, Verification*. J. Geophys. Res., 1999. **104**: p. 7649–7666.
12. Eckart, C. *The propagation of gravity waves from deep to shallow water*. 1952. USA: Proceedings of the NBS Semicentennial Symposium on Gravity Waves.
13. Dingemans, M., *Water Wave Propagation Over Uneven Bottoms*. Vol. 13. 1997, Delft: World Scientific.
14. Randall, D., *The Shallow Water Equations*. 2006, Colorado State University: Fort Collins.
15. Tu, J., G. Heng Yeoh, and C. Liu, *Computational Fluid Dynamics: A Practical Approach*. 2008, Burlington: Elsevier.
16. Kim, M.H., et al., *Fully Nonlinear Multidirectional Waves by a 3-D Viscous Numerical Wave Tank*. J. Offshore Mech, 2001. **123**(3): p. 124–133.
17. Park, J.C., et al., *Numerical reproduction of fully nonlinear multi-directional waves by a viscous 3D numerical wave tank*. Ocean Eng., 2004. **31**(11–12): p. 1549–1565.
18. Koo, W. and M.H. Kim, *Freely floating-body simulation by a 2D fully nonlinear numerical wave tank*. Ocean Eng, 2004. **31**(1): p. 2011–2046.
19. Sun, H. and O.M. Faltinsen, *Water impact of horizontal circular cylinders and cylindrical shells*. Appl. Ocean Res., 2006. **28**(5): p. 299–311.
20. Ning, D. and B. Teng, *Numerical simulation of fully nonlinear irregular wave tank in three dimension*. Int. J. Numer. Methods Fluids, 2007. **53**: p. 1847–1862.
21. Ning, D., et al., *Numerical simulation of non-linear regular and focused waves in an infinite water-depth*. Ocean Eng., 2008. **35**(8-9): p. 887-899.

22. Yan, H. and Y. Liu, *An efficient high-order boundary element method for nonlinear wave-wave and wave-body interactions*. J. Comput. Phys., 2011. **230**(2): p. 402-424.
23. Wu, G.X. and Z.Z. Hu, *Simulation of nonlinear interactions between waves and floating bodies through a finite-element-based numerical tank*. Ser Math. Phys. Eng. Sci., 2004. **460**(2050): p. 2797–2817.
24. Hadzic, I., et al., *Computation of flow-induced motion of floating bodies*. Appl. Math. Model., 2005. **29**(12): p. 1196–1210.
25. Turnbull, M.S., A.G.L. Borthwick, and R. Eatock Taylor, *Wave-structure interaction using coupled structured-unstructured finite element meshes*. Appl. Ocean Res., 2003. **25**(2): p. 63–77.
26. Agamloh, E.B., A.K. Wallace, and A. Von Jouanne, *Application of fluid-structure interaction simulation of an ocean wave energy extraction device*. Renewable Energy, 2008. **33**(4): p. 748–757.
27. Sriram, V., S.A. Sannasiraj, and V. Sundar, *Simulation of 2-D nonlinear waves using finite element method with cubic spline approximation*. J. Fluids Struct., 2006. **22**(5): p. 663-681.
28. Contento, G., *Numerical wave tank computations of nonlinear motions of two-dimensional arbitrarily shaped free floating bodies*. Ocean Engineering, 2000. **27**(5): p. 531-556.
29. Mousaviraad, S.M., P.M. Carrica, and F. Stern, *Development and validation of harmonic wave group single-run procedure for RAO with comparison to regular wave and transient wave group procedures using URANS*. Ocean Engineering, 2010. **37**(8-9): p. 653-666.
30. LIANG, X.-f., et al., *Numerical Simulation of Irregular Wave-Simulating Irregular Wave Train, Journal of Hydrodynamics*. Journal of Hydrodynamics, 2010. **22**(4): p. 537-545.
31. Lal, A. and M. Elangovan, *CFD Simulation and Validation of Flap Type Wave-Maker*. World Academy of Science, Engineering and Technology, 2008. **46**(1): p. 76-82.
32. Liu, G.R. and M.B. Liu, *Smoothed Particle Hydrodynamics: a meshfree particle method*. 2003, London: World Scientific Publishing Co. Pte. Ltd.
33. Malalasekera, H., *An Introduction to Computational Fluid Dynamics: The Finite Volume Method*. 1995, New York: John Wiley & Sons Inc.
34. Chorin, A., *Numerical Solution of the Navier-Stokes Equations*. Mathematics of Computation, 1968. **22**(104): p. 745-762.
35. Hirt, C. and B.D. Nichols, *Volume of fluid (VOF) method for the dynamics of free boundaries*. Journal of Computational Physics, 1981. **1**(39): p. 201-225.
36. Anbarsooz, M., M. Passandideh-Fard, and M. Moghiman, *Fully nonlinear viscous wave generation in numerical wave tanks*. Ocean Engineering, 2013. **59**(1): p. 73-85.
37. *Solution methods for the Incompressible Navier Stokes Equations*. 2012.
38. *ANSYS CFX Release 13*. 2011, -: ANSYS-Inc.
39. Andersson, H.I., *Introduction to Turbulence Modeling*. 1988, Norwegian Institute of Technology: Trondheim.
40. Menter, F., *Two-equation eddy-viscosity turbulence models for engineering applications*. AIAAJournal, 1994. **32**: p. 269-289.

41. Dean, R.G. and R.A. Dalrymple, *Water Wave Mechanics for Engineers and Scientists*. 2000, River Edge, NJ: World Scientific.
42. Miche, M., *Le pouvoir reflechissant des ouvrages maritimes exposes a l'action de la houle*. translated by Lincoln and Chevron, 1951. **Series 3**(Berkeley, Wave Research Laboratory): p. 285-319.
43. Madsen, O., *Waves Generated by a Piston-Type Wavemaker*. US Army Coastal Engineering Research Center, 1960: p. 589-607.
44. Morison, J.R., *The Force Distribution Exerted by Surface Waves on Piles*. 1950, University of California: Berkeley, California.
45. Havn, J., *Wave Loads on Underwater Protection Covers*. 2011, Norwegian University of Science and Technology (NTNU): Trondheim, Norway.
46. Lambert, R.J., *Development of a Numerical Wave Tank Using OpenFOAM*. 2012, Universidade de Coimbra: Coimbra, Portugal.
47. Stanley, J. *Development of a two dimensional numerical wave tank*. 2012. Canada: Eighth Mechanical Engineering Graduate Students Conference.
48. Zullah, M.A. and Y.-H. Lee, *Performance evaluation of a direct drive wave energy converter using CFD*. *Renewable Energy*, 2013. **49**(1): p. 237-241.
49. Prasad, D., M.R. Ahmed, and Y.H. Lee. *Performance Studies on a Direct Drive Turbine for Wave Power Generation in a Numerical Wave Tank*. 2012. Jeju island, Korea: Asian Wave and Tidal Conference Series.
50. Cruz, J., *Ocean Wave Energy: Current Status and Future Perspectives*. 2007: Springer.
51. Moghiman, M., M. Passandideh-Fard, and M. Anbarsooz, *Fully Nonlinear Viscous Wave Generation in Numerical Wave Tanks*. *Ocean Engineering*, 2013. **59**: p. 73-85.
52. Techet, A.H., *Morrison's Equation*. 2004.